Hard Carbons as Anode Materials for Lithium-ion Batteries

by

Yinghu liu

B.Sc., Peking University, 1990

A THESIS SUBMITTED IN PARTIAL FULFILLMENT OF

THE REQUIREMENTS FOR THE DEGREE OF

MASTER OF SCIENCE

in the Department

of

Physics

©   Yinghu Liu   1995

SIMON FRASER UNIVERSITY

July 1995

Approval

Name: Yinghu Liu

Degree: Master of Science

Title of Thesis: Hard Carbons as Anode Materials for Li-ion Batteries

Examining Committee:

Dr. John Bechhoefer
Chairperson

Dr. Jeff R. Dahn
Senior Supervisor

Dr. George Kirczenov
Supervisor

Dr. Steve Holdcroft
Supervisor

Dr. Robert Frindt
Internal Examiner

Date Approved: 11 July 1995

PARTIAL COPYRIGHT LICENSE

I hereby grant to Simon Fraser University the right to lend my thesis, project or extended essay (the title of which is shown below) to users of the Simon Fraser University Library, and to make partial or single copies only for such users or in response to a request from the library of any other university, or other educational institution, on its own behalf or for one of its users. I further agree that permission for multiple copying of this work for scholarly purposes may be granted by me or the Dean of Graduate Studies. It is understood that copying or publication of this work for financial gain shall not be allowed without my written permission.

Title of Thesis/Project/Extended Essay

Hard Carbons as Anode Materials for Lithium-ion Batteries.

_____

_____

_____

Author:_____
   (signature)

   Yinghu Liu
   (name)

   (date)   Aug. 2, 1995

Acknowledgments

Abstract

Usually, a lithium transition metal oxide is used for the cathode and a carbonaceous material for the anode of a lithium-ion cell. Here, we study the performance of hard carbons as anode materials.

We made our own carbonaceous materials (or carbons for simplicity) by pyrolyzing epoxy novolac resins (DEN 438), which are highly crosslinked materials. First hardened by phthalic anhydride at 120°C for 24 hours, the resins were pyrolyzed in an argon atmosphere at 1000°C to form carbons.

X-ray Diffraction was used to investigate the structure of the carbons. Different pyrolyzing conditions (heating rate, argon flow rate, etc.) can alter certain features of the X-ray pattern, but in all cases, the (002) peak was broad and weak. The (002) peak was found on a large background due to the presence of single-layer carbon sheets.

It is hard to fit the X-ray diffraction pattern of hard carbon. But there is a close connection between the shape of the 002 peak and the microstructure of the carbon. A broader and weaker 002 peak indicates more monolayer microstructure in the material. We defined an empirical parameter R to describe the stacking properties of the carbon layers. Cells with these hard carbons as cathodes and lithium metal as anodes have capacities as high as 570 mAh/g ($Li_{1.5}C_6$),

while for graphite, the value is only 372mAh/g (LiC_6).   Therefore, these hard carbons are promising candidates as anode materials for lithium-ion batteries.

After carefully studying several groups of samples, we found that the capacity is negatively correlated to R; that is the capacity is the highest when the 002 peak is the weakest and the monolayer microstructure is dominant.

The high capacities of these materials indicate a mechanism for lithium insertion different from that of lithium intercalation into graphite.   We propose that instead of forming an intercalated phase as in graphite (see figure 1.3.1),   lithium atoms are adsorbed on both sides of the single carbon layers due to the monolayer and nanoporous nature of the materials (see figure 1.3.3).

Contents

4. Electrochemical Tests

4.1 Introduction   44

4.2 Cell Construction   45

4.3 Cell Testing   47

5. Summary and Suggestions for Future Work

5.1 Mechanisms of Lithium Intercalation into Different Carbonaceous Materials   58

5.2 Practical Considerations   61

5.3 Suggestions for Future Work   62

List of Figures

List of Tables

Chapter 1   Introduction

1.1 Li-ion Batteries using Carbon-based Materials as Anodes

Intercalation is the reversible insertion of guest atoms into host solids, provided the structure of the host is not significantly altered. In the mid-seventies it was realized that the reversibility of inserting and removing the guest from the host could be exploited to make rechargeable or secondary batteries.[1] The most popular guest element initially used for rechargeable batteries was lithium because lithium metal electrodes were light, lithium batteries had high voltage, and lithium could be efficiently electroplated in some organic solvents.

Secondary lithium batteries operating at room temperature offer three main advantages compared to conventional technologies.[2]

> 1) Higher energy density (up to 100 Whr/kg)
>
> 2) Higher cell voltage (up to 3.5 volts per cell)
>
> 3) Longer shelf life (up to 5 to 10 years)

During the 1970's and 80's, almost all work on secondary Li batteries centered on the use of intercalation compounds as the positive electrode and metallic Li or Li-alloys as the negative electrode. Lithium atoms have lower chemical potential in air stable intercalation compounds than in Li metal or Li-alloys. Therefore, Li is intercalated into the host compounds during the

discharge of lithium intercalation cells and forced back to the metal or alloy anode during recharge. Fig. 1.1.1 illustrates the discharge process schematically.

In spite of the many advantages as mentioned above, batteries with metallic Li anodes have proven to have serious safety problems.[3, 4, 5] Therefore a new chemistry called the 'rocking chair' or 'Lithium-ion' battery[6, 7] has drawn more and more attention since the late 1980's. In this approach, two intercalation compounds, each highly reversible, are used as electrodes.

The high energy density of Li-ion cells arises from two factors: the large potential difference between the electrodes and the large specific capacity of the electrode materials. Therefore, the choice of materials to be used for the negative electrode in Li-ion batteries is restricted to those with a chemical potential reasonably close to that of Li metal. Fig. 1.1.2 shows why carbonaceous materials are clearly the most promising candidates. The cost, availability, performance and chemical potential versus Li-metal of carbon-based materials are all acceptable for practical cells.

One piece of evidence for this is that $LiCoO_2$/carbon cells[6] are now commercially available. The cells have about twice the energy density of Ni-Cd and Ni-Metal Hydride cells and are hence preferred for portable applications. There has been a lot of work on $LiNiO_2$/carbon[7] and $LiMn_2O_4$/carbon[8] cells as well.
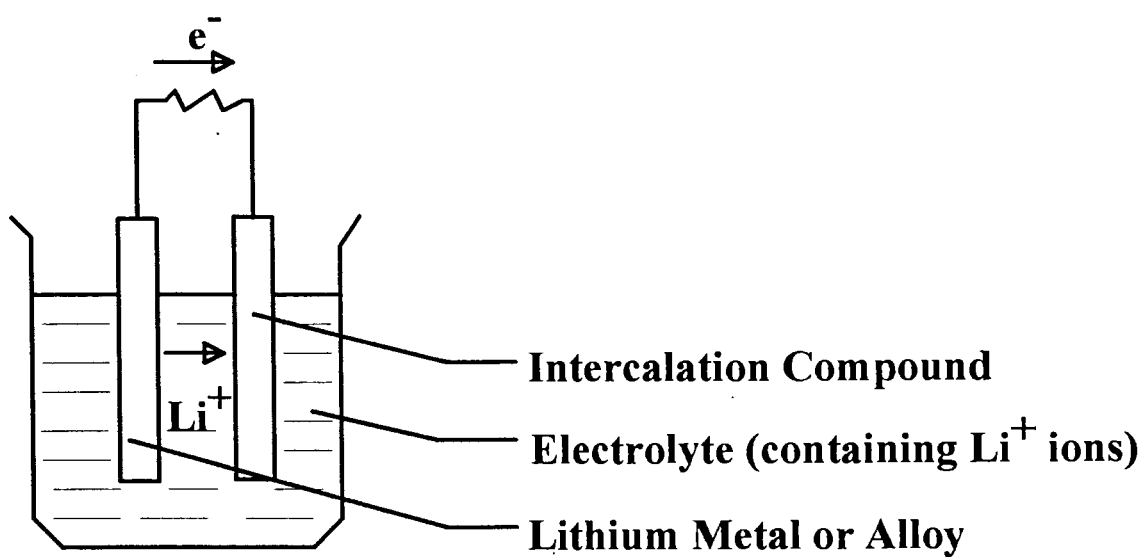
Fig. 1.1.1 Schematic view of a Li intercalation cell

$Li_{1-y}NiO_2$
$Li_{1-y}CoO_2$

Li_xMnO_2

Li_xTiS_2

Li_xMoS_2

Li_xMoO_2

$0<x<1.0$
$0<y<1.0$

Li_xWO_2

Li_xCoke

$Li_xGraphite$
$Li\ metal$

0	-1	-2	-3	-4	-5	-6eV (vs. Li metal)
3.04	2.04	1.04	0.04	-0.96	-1.96	-2.96eV (vs. SHE)
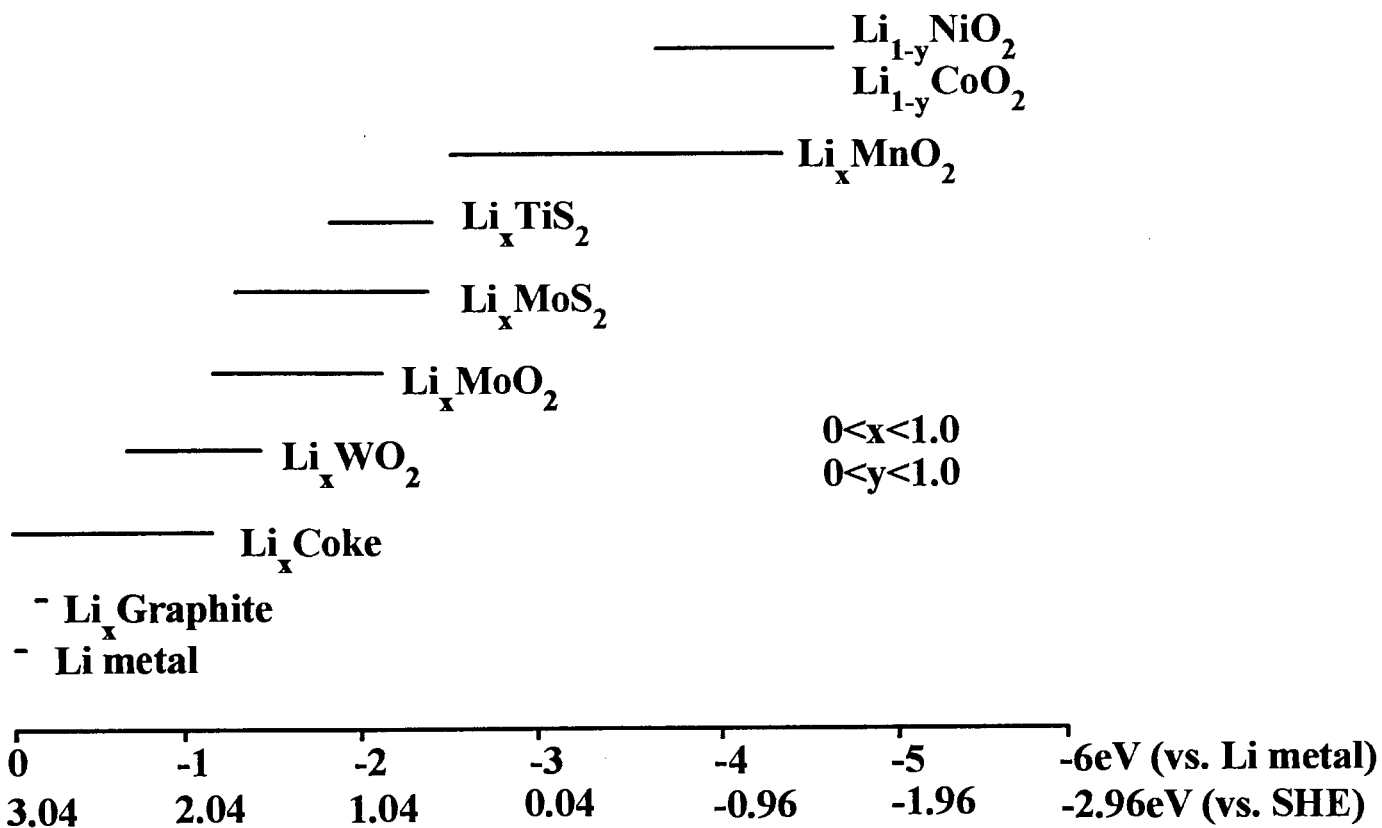
Fig 1.1.2 Chemical potential ranges of intercalated Li in a variety of compounds

1.2 Carbonaceous Materials

1.2.1 Basic Structural Units

It is well-known that there are two types of carbon-carbon bonds in solid carbons. One is the tetrahedral bond (sp^3), as in diamond; the other is the trigonal bond (sp^2), as in graphite.[9] In the carbonaceous materials we will consider in this thesis, most of the carbon atoms are in sp^2 bonds. However, in highly disordered carbonaceous materials, there might exist a small amount of tetrahedral bonds in highly stressed or crosslinked areas.

All carbonaceous materials prepared from organic precursors are initially made of similar microstructures which are formed in specific arrangements[10]. As organics are heated they decompose and form small planar aromatic structures (Fig. 1.2.1) consisting of less than 10-20 hexagonal rings; we call these graphene sheets here. These are sometimes stacked in a more or less parallel way in groups of two to five units. These structures are sometimes called 'basic structural units'. If some of these elemental units align edge to edge and face to face with parallel aromatic sheets, then the 002 Bragg peak of the x-ray diffraction pattern will be observed.[11] The size of such clusters of oriented units is an important indication of the carbon structure. The clusters can range from less than 5 nm to larger than 200 nm. They can even form crumpled or flat lamellae as big as the size of the crystallite.
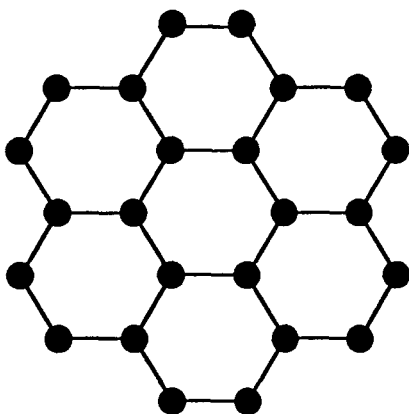
Fig 1.2.1 Illustration of a small aromatic
layer made of 7 benzene rings
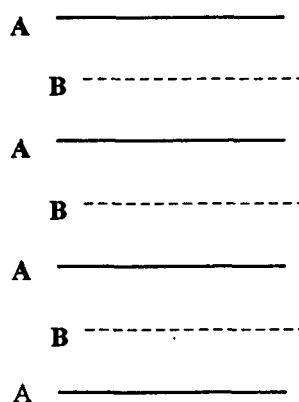
Fig 1.2.2 The ABAB.. stacking structure
of hexagonal (2H) graphite

1.2.2 Soft Carbons and Hard Carbons

Low temperature disordered carbons are usually split into two classes, soft carbon (Fig. 1.2.3)

and hard carbon (Fig. 1.2.4), according to their graphitizability. Soft carbons refer to the carbons

that can be turned into graphite (see figure 1.2.2) after heat treatment at 2800°C or higher, while

hard carbons remain disordered after the same treatment. Some results show that under high

pressure (5kBar), some hard carbons can be changed into soft carbons at 1800°C[12].

Most of the basic structural units of soft carbons are multilayers and have a preferred orientation

(Local molecular orientation) for a large region. In hard carbons, however, more monolayer

structural units are found, and they are not as ordered as in soft carbons. The carbon structure

greatly influences the intercalation of lithium as we will see later in section 1.3, and hence affects the selection of carbons to be used in Li-ion cells.

——— Small Aromatic Layer

Fig 1.2.3 The local molecular
          orientation of soft carbon

Fig 1.2.4 The microstructure
          of hard carbon

1.2.3 Production

There are hundreds of carbons commercially available, and organic compounds are the main and almost exclusive raw materials for the production of artificial carbons. By pyrolysis in inert gas, these carbon compounds are converted to solid carbon as the main product and to different volatile compounds as by-products.[13] Later in chapter 2, I will show how different conditions of pyrolysis change the structure of the resulting carbons.

1.3 Lithium Intercalation in Carbonaceous Materials

1.3.1 Lithium Intercalation into Graphite

Much of the early work on lithium intercalation into carbons has been performed on Highly Ordered Pyrolytic Graphite (HOPG) which is very well graphitized. The early work focused on the study of the staged phases that form in lithium intercalated graphite.[14] A stage n structure is a sequence of n graphite layers and one intercalate layer as shown schematically in figure 1.3.1. Near room temperature the following single phases were observed, stage-4, stage-3, liquid-like stage-2 (called 2L), stage-2, stage-1. The largest amount of lithium which can be intercalated into graphite is achieved using stage-1 LiC_6.

Graphite   Stage 1   Stage 2   Stage 3

- - - - - - Lithium Layer   ——————— Carbon Layer
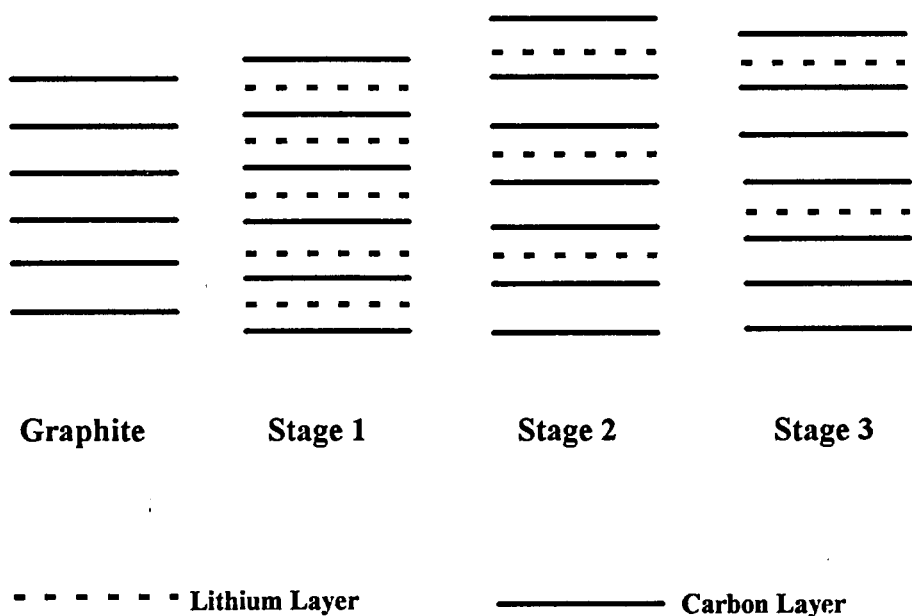
Fig. 1.3.1 Some staged phases of lithium intercalated graphite

The in-plane structure of stage-1 LiC_6 is shown in Fig.1.3.2. Li atoms reside in the center of the Van der Waals gap centered on the carbon hexagons of the AAAA stacked carbon sheets. (The carbon layers shift from ABAB... to AAAA... stacking when Li is intercalated.) Every Li atom is

located on a hexagonal superlattice with a lattice constant $\sqrt{3}$ times as large as the graphite a-axis, such that no pairs of Li atoms occupy nearest-neighbor sites. In such a structure there is exactly one Li for every 6 carbon atoms. Under high temperature (280°C) and pressure (50kBar), more than 1 Li can be intercalated for every 6 carbon atoms[15] by forcing some lithium atoms to take nearest-neighbor positions.
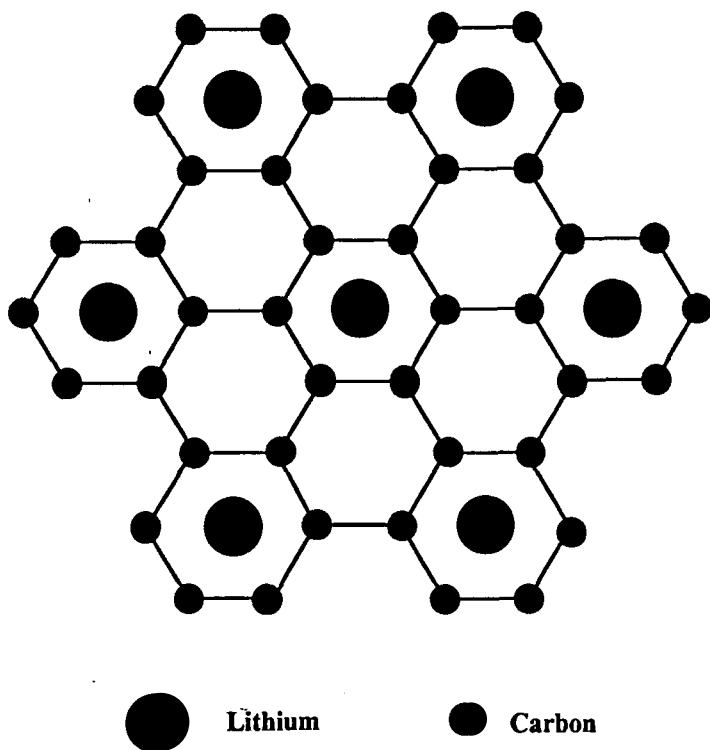
● Lithium   ● Carbon

Fig 1.3.2 The in-plane structure of LiC$_6$

1.3.2 Lithium Intercalation into Soft Carbons

Very little fundamental work on intercalation in disordered carbons has been carried out because intercalation showing staged phases is facilitated by a high degree of structural order of the graphite host material and is retarded by defects, structural imperfections or disorder. Good staging fidelity is achieved only in hosts with a high degree of structural perfection.[16]

A commercial Li-ion cell anode will not be made of HOPG, but instead of a low-cost powdered carbon or graphite. Therefore, we must understand the mechanism of lithium intercalation into these disordered carbons. Dahn et al [17] have done careful studies of the intercalation of lithium in soft carbons and verified that staged phases do not form at any x in Li_xC_6 for petroleum coke. They proposed a phenomenological model which explains this effect. For heated soft carbons, the highest reversible capacity occurred at low (~700°C) and high (~2800°C) heat-treatment temperature[18], but the capacity was never bigger than that of graphite (except for hydrogen containing carbons[19]). The effect of turbostratic disorder (translational shifts between adjacent graphene sheets) in soft carbons on the intercalation of lithium has been carefully studied by Zheng et al.[20]

1.3.3 Lithium Intercalation into Hard Carbons

Although lithium-ion cells have much higher energy density than other types of rechargeable batteries available now, there is considerable marketing incentive to increase the energy density of

Li-ion cells still further, so that portable devices can be further miniaturized. As mentioned above, increases to the specific capacity of the electrode materials leads to increases in the energy density of lithium-ion cells. Our attempt to intercalate lithium into hard carbons is only one of many efforts focusing on increasing the specific capacity of the anode materials.

For example, Way and Dahn[21] showed how the incorporation of electron acceptors substitutionally for carbon in the graphite structure leads to increases in specific capacity. They obtained reversible capacities, Q_r, as high as 440 mAh/g with boron-substituted carbons. Wilson and Dahn[22] showed that pyrolyzed siloxane polymers could also have specific capacities near 600 mAh/g.

The research group at Sony[23] showed how pyrolyzed furfuryl alcohol could have Q_r as large as 450 mAh/g. Mitsubishi Gas Chemical[24] has developed a carbonaceous material with Q_r = 500 mAh/g. The Sony and Mitsubishi Gas materials are prepared from precursors which lead to non-graphitizable or hard carbons when heated. This means that the precursors are chosen such that cross-linking between graphene sheets prevents the ordered stacking of layers in the graphite structure, as the materials are heated. It is our opinion that when poorly stacked layers are present, it may be possible to adsorb lithium onto the surfaces of each side of the layers. These surfaces are found within the carbon particles, on the atomic scale (see figure 1.2.4).

In graphite, because the layers are well stacked and parallel, intercalation of lithium to a composition of LiC_6 (or 372 mAh/g) leads to one intercalated layer of lithium per graphene sheet.

In materials with poorly stacked layers, unshared lithium layers could possibly be found on each side of the graphene sheets, as shown in Fig 1.3.3, leading to compositions near Li_2C_6 (740mAh/g). Therefore we believe that an important factor is the number of single-layer graphene sheets in the material. The use of non-graphitizable precursors like those used by Sony leads naturally to such materials. It is our goal to test this idea by preparing carbons with a large amount of single graphene layers.

|⎯⎯⎯⎯⎯| 1 nm

⎯⎯⎯⎯⎯⎯   Carbon Layer

●   Lithium atom
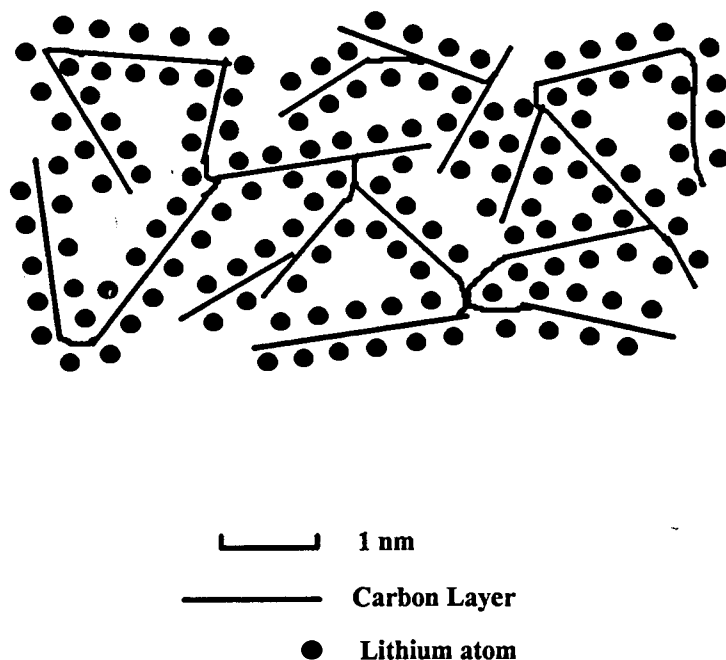
Fig 1.3.3 Lithium insertion into a hard carbon with mainly monolayer microstructure

Chapter 2   Materials Preparation

Our starting materials are Dow epoxy novolac resin (D.E.N.438) and phthalic anhydride which is a curing agent for the resin. The preparation of hard carbons involves two consecutive steps, the hardening of the epoxy novolacs by the curing agent and then the pyrolysis of the cured resin systems.   The resins become hard during the curing process because of the high density of crosslinks formed in the system.

2.1 Hardening of Epoxy Novolac Resins

2.1.1 Epoxy Novolac Resins

Fifty years ago, epoxy resins were introduced commercially, and since then their variety and applications have never stopped growing. Although epoxy resins are not an especially large-volume commodity compared with some other classes of plastics, they are one of the most versatile plastics. These resins are used in literally hundreds of applications. It should therefore not come as a surprise if we have found another application for this very popular plastic. Epoxy resins are currently priced at US$2.50 per pound for bulk purchases (55 gallon drum or more).

These resins are characterized by the reactive oxirane ring [$-\overset{\overset{O}{\diagup\diagdown}}{CH-CH}-$], also called the epoxide functional group, which can react with hardening agents or can be catalytically homopolymerized to form a crosslinked polymeric structure.

D.E.N. 400 series epoxy novolac resins from the Dow Chemical company are viscous semi-solid materials with multiple epoxide functional groups (see Fig. 2.1.1). Their viscosity is reduced to manageable levels by heating to about 100°C. The multifunctionality of epoxy novolacs leads to a high crosslink density in the polymeric structure after the resins are hardened. The hardened systems are easier to handle than pure resins and can be pyrolyzed under different conditions to form a series of hard carbons with a wide range of structural properties (see chapter 3).
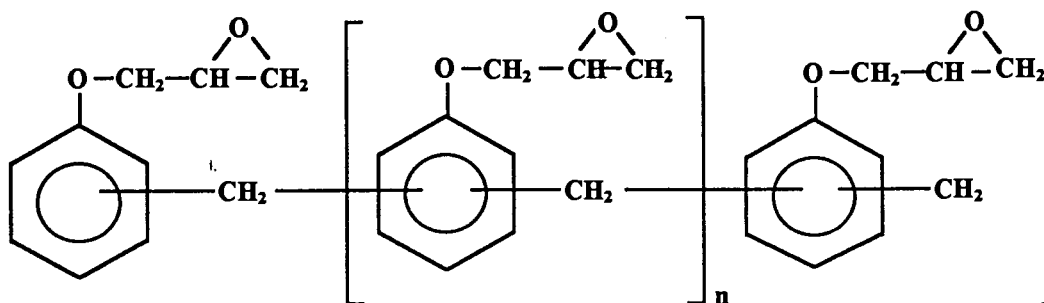
D.E.N. 400 Epoxy Resin series, D.E.N. 438   n=1.6

Fig. 2.1.1 Molecular formula of epoxy novolac resins

2.1.2 Hardening Agents

There are several groups of hardening agents for epoxy novolacs[25][26], most of which contain nitrogen. Based on earlier work which suggested that nitrogen is detrimental[27], we chose phthalic anhydride as the curing agent to avoid introducing any nitrogen into the final carbon products. The anhydride functional group is shown below, together with the molecular formula of phthalic anhydride. Phthalic anhydride is a white powder with a melting point of 128°C. It is miscible with D.E.N. 438 at 90°C.

Phthalic Anhydride   Anhydride Group
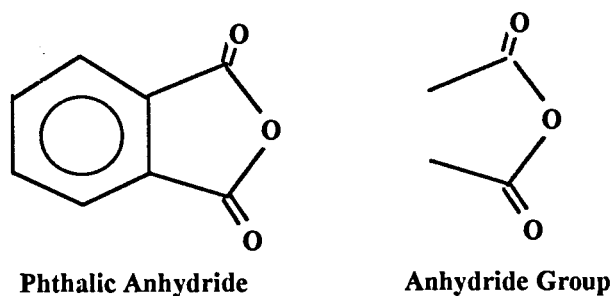
Fig. 2.1.2   Molecular formula of the curing agent

2.1.3 Reactions of the Epoxy Resins with Anhydride

The reactions of anhydrides with epoxy groups are complex, with several competing reactions capable of taking place. According to the manual from the DOW company[25], the three most important reactions are:

i) The opening of the anhydride ring with an alcoholic hydroxyl to form the monoester:
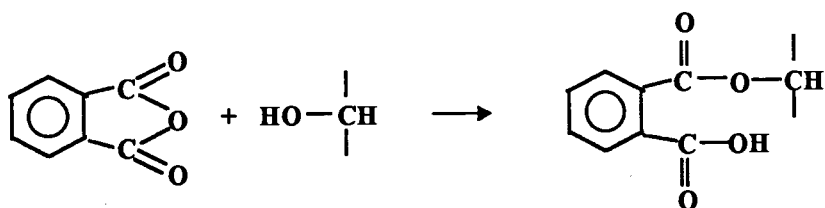
ii) Subsequent to (i), the nascent carboxylic groups react with the epoxide to give an ester linkage:
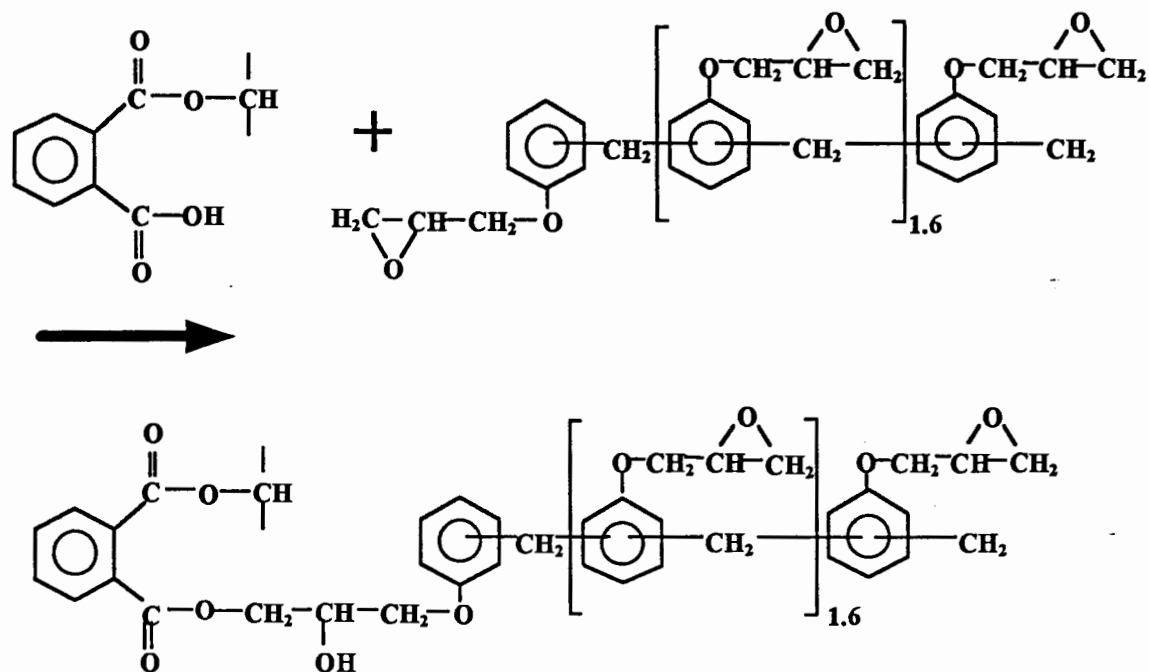
iii) The epoxide groups react with nascent or existing hydroxyl groups, producing an ether linkage:

15
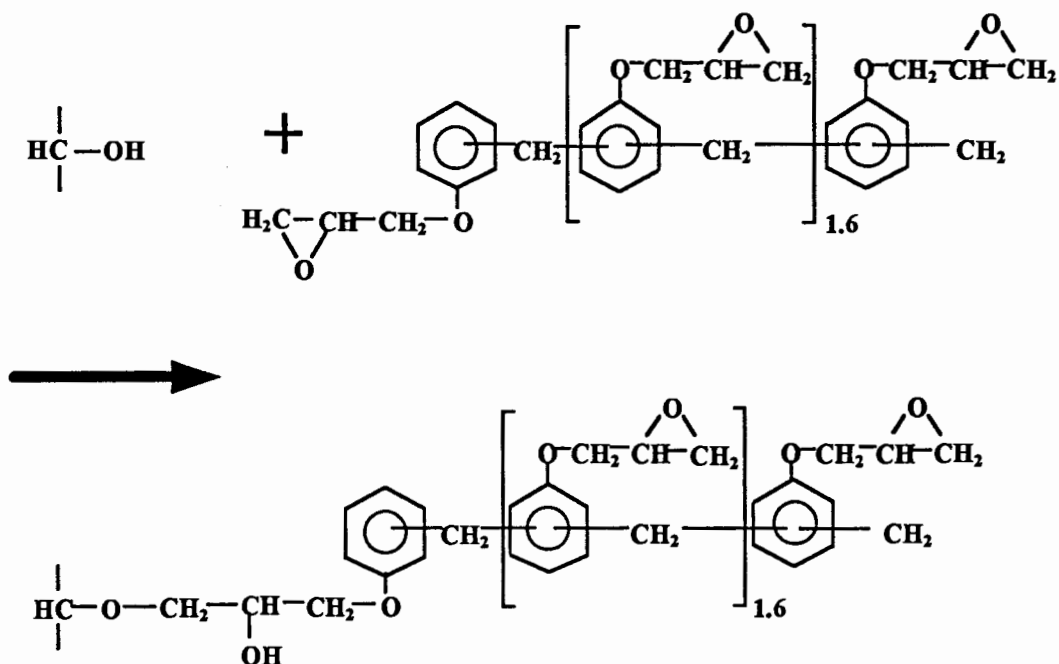
The new hydroxyl groups formed in step ii) and iii) then react with other epoxide groups to form crosslinkages between molecules. For example,

Crosslinkage
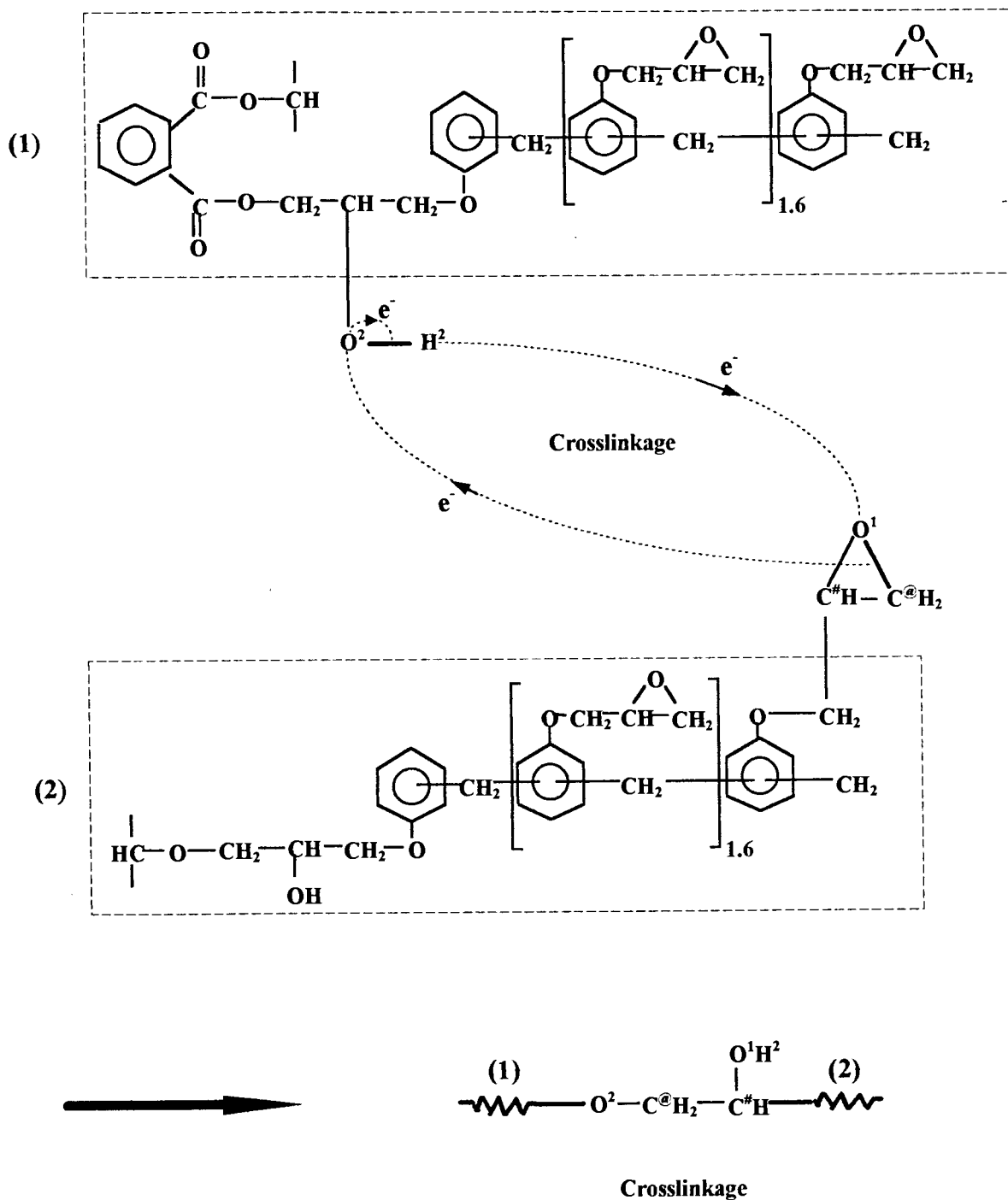
As a result of the competition among the reactions and the multifunctionality of the novolac resin, the equivalent[a] ratio of anhydride to epoxy is not critical because iii) can actually happen without the presence of anhydride. The ratio can vary from 0.5 to 0.9 equivalents of anhydride per equivalent of epoxy and is determined experimentally to achieve desired properties. In our case, we wanted to try different hardening and pyrolysis conditions to make carbons with different stacking properties.

The curing reactions need to be initiated by alcoholic hydroxyl groups. We did not add any acids or bases to help form such hydroxyl groups because we learned from the Dow Chemical company that polyglycol was used during resin production and that there is a small amount of it in the resin which is enough to start the reaction chain.

The mass ratio of phthalic anhydride to D.E.N. 438 was as large as 60% for our samples; that is, the equivalent ratio was as large as 1.07. The curing procedure was simple. The ingredients were first weighed and placed in a nickel-foil container. This was then placed in a oven at 90°C for about 1.5 hours to melt and mix thoroughly. Then the temperature of the oven was adjusted to 120°C and the mixture was heated overnight. Some of the samples were cured at 170°C for about 10 hours after mixing, in which case the hardened resins were more brittle and easier to grind into powder.

---

[a] Equivalent Weight (EW) = Mol Weight / Number of Functional Group
    D.E.N. 438   EW = 157,   Phthalic Anhydride   EW=88
    Equivalent = Weight / Equivalent Weight

The cured resins were then either broken into small bricks of about 0.5 cm^3 or ground into powders of fine particles less than 180μm in diameter. These chunks and powders were the precursors of the hard carbons.

2.2 Pyrolysis of Hardened Resins

2.2.1 General Rules for Polymer Pyrolysis

Pyrolysis is the decomposition process which occurs at high temperature in vacuum, inert gas, or other nonreactive atmospheres. Although there has been a tremendous effort on this subject, the physical changes and chemical reactions taking place during pyrolysis are not yet understood thoroughly. Our goal is to make hard carbons with monolayer microstructures, so we need only follow some general rules concerning the pyrolysis of polymers from Fitzer's work in the 1970's[13].

When polymers are pyrolyzed, reactions take place initially within the carbon-carbon chain. These intermolecular reactions result in one of three possibilities:

i) The chains degrade into small molecules and the products are evolved as gases leaving little or no carbon behind. An example of this behavior is shown by polyethylene.

ii) The chains collapse to form aromatic lamellae and so move into a semiliquid phase from which the lamella stack above each other to form spherullitic liquid crystals - so called 'mesophase'. The result is a crystalline anisotropic coke or soft carbon which on heating to 2700°C will produce graphitic materials. An example of this behavior would be the heating of polyvinyl chloride.

iii) The chains remain intact and merely coalesce with neighbors. The materials do not pass through a semiliquid state. The final char is isotropic if the precursor is isotropic and can be anisotropic if the precursor material is anisotropic. In both cases the materials are not graphitizable when they are heated to 2700°C and are called hard carbons. An example of a material which behaves like this is polyvinylidene chloride (used in saran wrap), which forms hard carbon.

The pyrolysis of hardened epoxy resins falls into the third category. There were no semifluid or fluid states which occurred during the process. This was verified by the fact that the carbons retained the same, but shrunken, shape as the precursors. It was later confirmed using X-ray diffraction that the carbons produced by pyrolyzing hardened epoxy novolacs were hard carbons. Only broad and weak 002, 100 and 110 Bragg peaks appeared on the x-ray patterns of these carbons. Further studies of these peaks showed that the carbons contain a large fraction of single layer microstructure which is a characteristic of hard carbons (see chapter 3).

The structure of the carbons produced by pyrolysis depend critically upon the chemical and physical conditions of the total pyrolysis process.

2.2.2 Characteristics of Pyrolyzed Resins

The chemical reactions which occur during pyrolysis are very complicated and I am not going to discuss them in detail here. Instead, I will briefly review the section in Dr. Fitzer's paper about the pyrolysis mechanism of several highly crosslinked polymers containing oxygen. As shown in section 2.1, the hardened resin systems belong to this category.

Based on experimental results and theoretical analysis, Fitzer and coworkers concluded that the mechanism of solid-state pyrolysis pertaining to highly crosslinked polymers distinguished itself from the liquid-state pyrolysis leading to planar sheets of polycyclic aromatics. The resulting aromatic sheets in the carbons will be translationally shifted (turbostratic) and angularly displaced, similar to how they existed previously in the crosslinked polymers. The carbons produced are more likely to be nongraphitizable under high-temperature heat treatment. On the other hand, the crosslinkages make the release of low-molecular-weight gas difficult and therefore lead to high carbon yield.

Apart from the chemical properties of the precursors, the physical kinetics of the pyrolyzing process also has a great influence on the carbon structure. Temperature, heating rate and pressure are three of the most important physical parameters of pyrolysis. We also found that the morphology of the precursor is another key factor in determining the microstructure of the carbons produced.

2.2.3 Experimental Procedure

The furnace used to pyrolyze the resins is shown in Fig. 2.2.1. The hardened resins were heated to 700°C-1000°C at different heating rates between 0.4 and 20°C/min in argon atmosphere. Both bulk and powdered precursors were used to test the effect of the morphology of the sample on the resulting carbon structure. Most of the samples were heated to 1000°C to reduce the content of impurities such as oxygen and hydrogen. Some samples were made at 700, 800, 900°C and 1100°C for comparison.
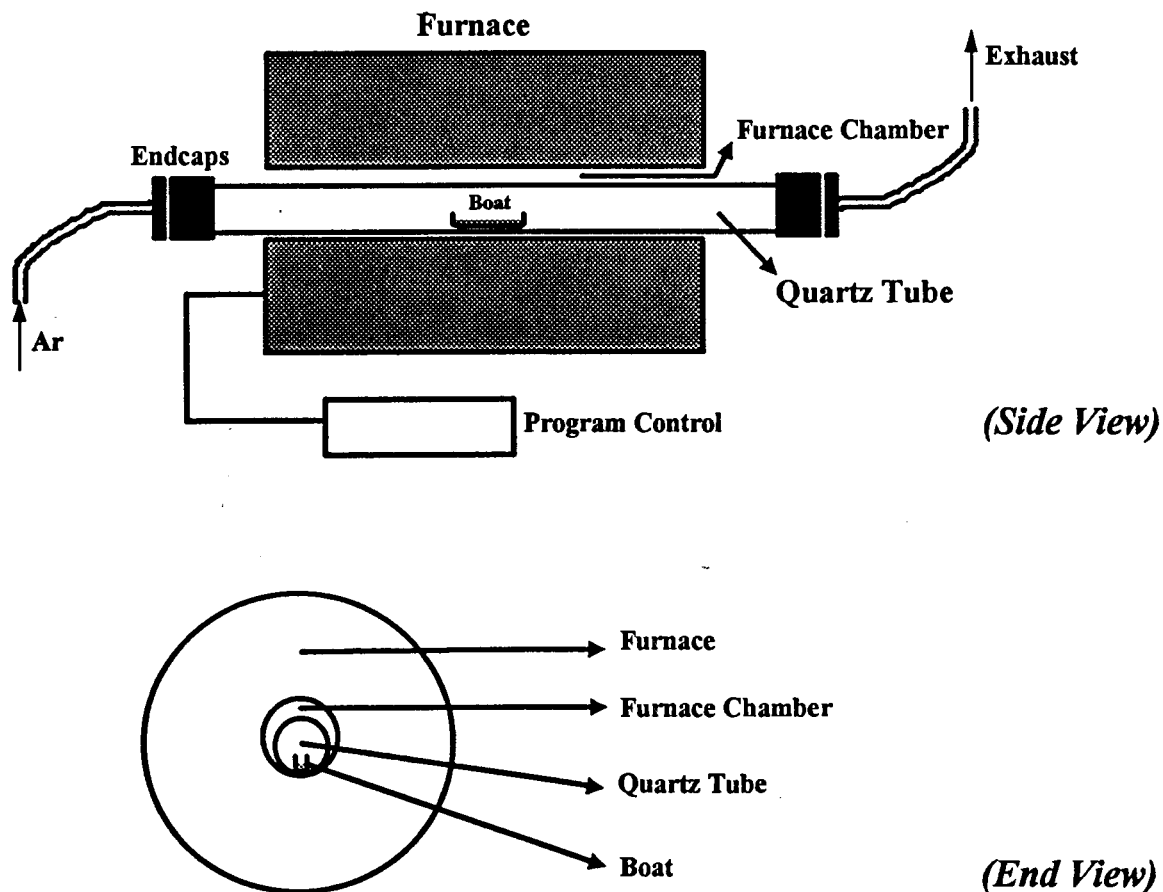
Fig. 2.2.1 Cross-sectional views of the pyrolyzing system

The bulk or ground hardened-resin was put into an alumina or nickel boat to be pyrolyzed inside a quartz furnace tube, which was within the furnace chamber. The tube was flushed with UHP-grade (99.999%) argon for 30 minutes to drive the air out before heating. Argon flowed through the tube during the pyrolysis process to remove the exhaust gasses. The heating rate, isothermal time and isothermal temperature (see Fig. 2.2.2) of heating were controlled by a temperature programmer. An illustrating temperature - time curve for a heating program is shown in Fig. 2.2.2. It took several hours for the furnace to cool down to 100°C. It was then opened and the quartz tube taken out. After the tube cooled to room temperature, the argon flow was switched off and the boat with the carbons inside was taken out.

The carbonaceous materials made were shiny gray bricks or black powders depending on the morphology of the precursors used. The materials were then weighed and ground into fine powders to be tested for compositional and structural properties. The results are summarized in chapter 3.
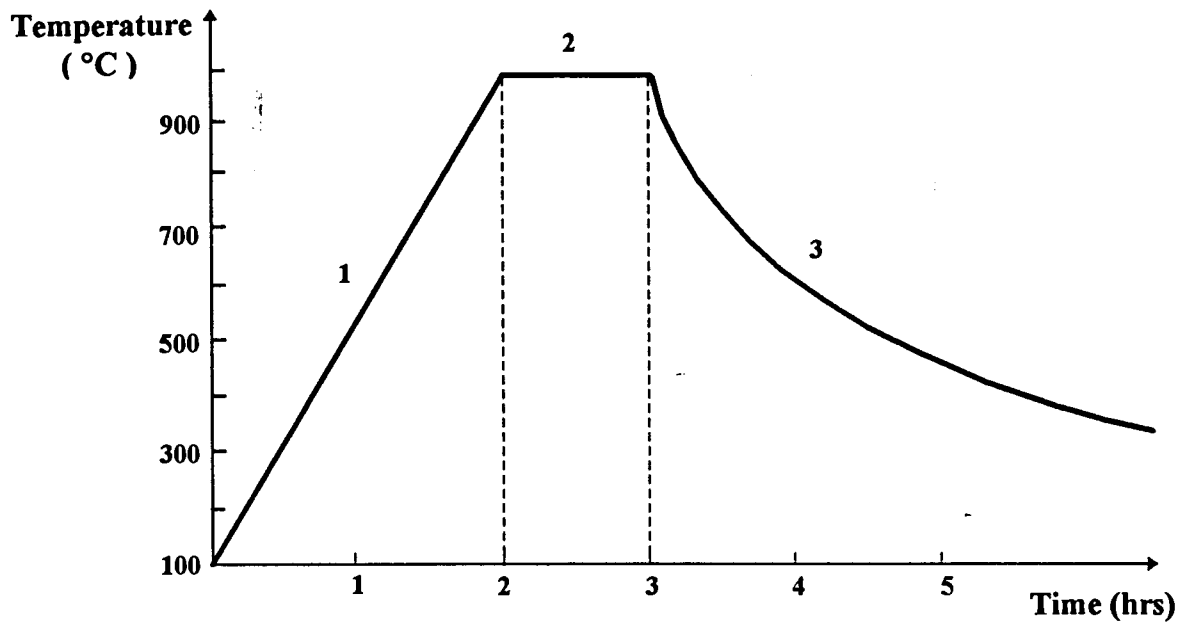
1) heating rate = 10°C/min
2) isotime = 60min, isotemp = 1000°C
3) cooling period

Fig. 2.2.2   Heating profile used in pyrolysis

Chapter 3   Compositional and Structural Examinations

3.1 CHN Analysis

CHN analysis is commonly used to measure the weight percent of carbon, hydrogen and nitrogen in various organic compounds. In this method, the samples are combusted and the amounts of carbon, hydrogen and nitrogen are determined by a gas chromatographic analysis of the combustion products. The analysis of our samples was done by Canadian Microanalytical Service (Delta, BC). The results (Table 3.1) are reported in weight percentage for each element and have a standard deviation of ±0.3%. Data in column 2 of Table 3.1 are the weight percent of phthalic anhydride in the hardened resin system. In the last column, we estimated the Hydrogen/Carbon (H/C) atomic ratio by taking the mass ratio of hydrogen to carbon for each sample and multiplying it by 12, which is the atomic mass ratio of carbon to hydrogen.

H/C atomic ratios were reduced significantly as the heat treatment temperature increased from 700°C to 1000°C (see Fig. 3.1.1). For samples made at 1000°C, CHN analysis showed that the carbon contents were greater than 93% and the hydrogen contents were less than 0.7% of the total sample weights. The H/C atomic ratios calculated for these samples were less than 0.09. The weight percentage of hardener (phthalic anhydride) and the heating rate did not affect the H/C atomic ratio considerably. The nitrogen content of all the samples was low. We did not analyze the oxygen content of these samples.
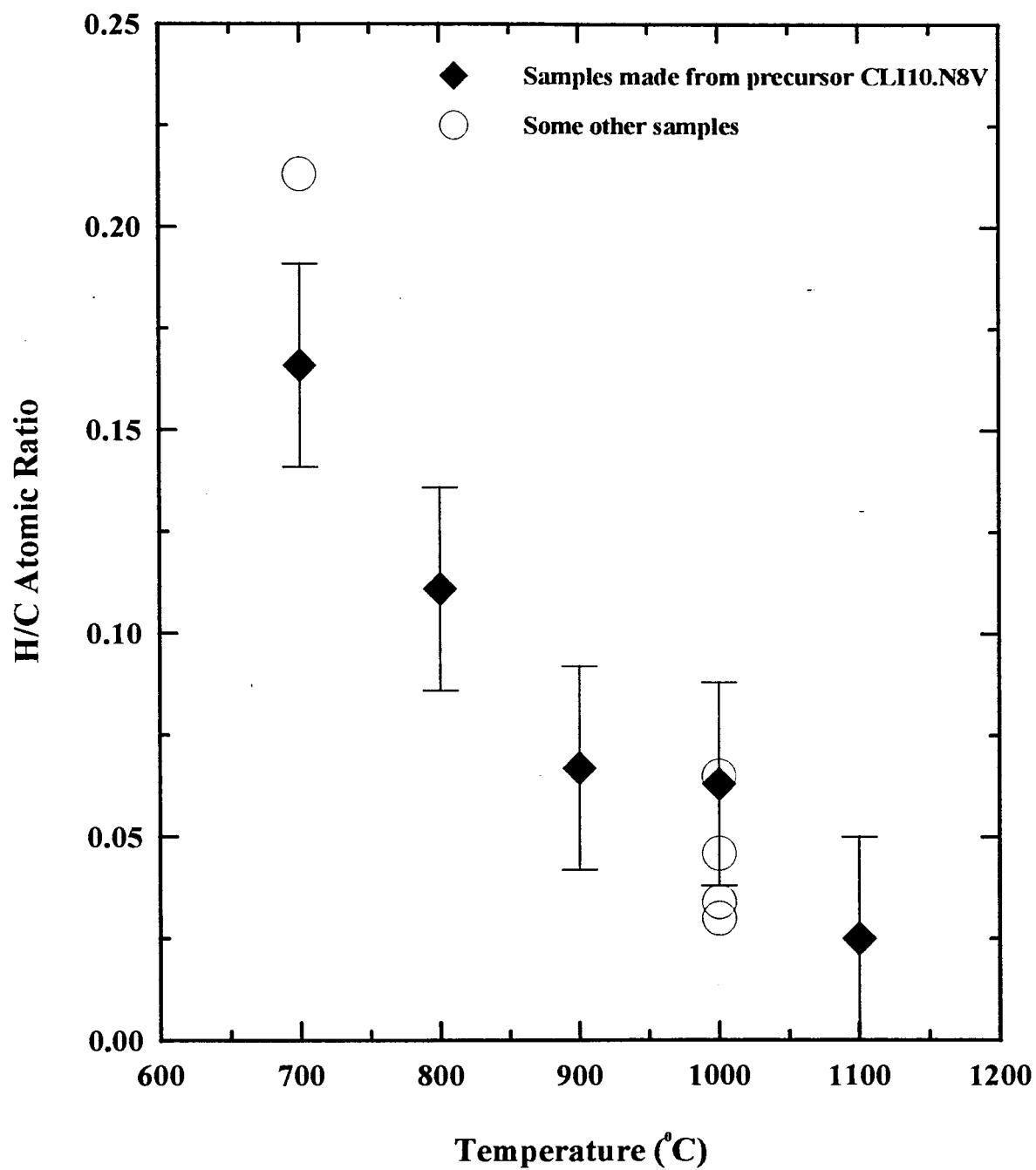
Fig. 3.1.1 The H/C atomic ratio versus pyrolysis temperature

Table 3.1 CHN Analysis Results

SAMPLE ID	$^{\$}$P.A.(%)	HEATING RATE(°C/min)	TEMP. (°C)	C(%)	H(%)	N(%)	H/C
CL10IA	11.4	10	1000	95.56	0.31	0.48	0.039
CL14IA	37.8	1	1000	95.69	0.52	1.05	0.065
CL11IA	37.8	2	1000	96.16	0.27	0.71	0.034
CL13IA	37.8	5	1000	94.74	0.36	0.23	0.046
CL12IA	37.8	10	1000	93.04	0.23	0.60	0.030
CL17IA	0.00	1	1000	95.41	0.26	0.46	0.033
CL17IC	14.8	1	1000	95.37	0.69	0.49	0.087
CL19IA	22.8	1	1000	95.59	0.43	0.65	0.054
*CL28IA	0.00	1	1000	95.47	0.17	0.21	0.021
*CL25IA	14.8	1	1000	95.06	0.40	0.64	0.050
*CL30IA	22.8	1	1000	95.37	0.38	0.67	0.048
*CL32IA	44.0	1	1000	95.78	0.38	0.30	0.048
CL38IB	14.8	$^{\#}$5,0.5,5	1100	97.25	0.20	0.18	0.025
CL45IA	22.8	20	700	93.27	1.29	LT.0.10	0.166
CL46IA	22.8	20	800	91.73	0.85	LT.0.10	0.111
CL46IB	22.8	20	900	93.39	0.52	LT.0.10	0.067
CL45IB	22.8	20	1000	95.24	0.50	0.19	0.063
CL63IA	14.8	20	700	94.15	1.67	LT.0.10	0.213

Note: $^{\$}$ Phthalic Anhydride. $^{\#}$ Heating rate was 0.5°C/min from 300°C to 600°C and 5°C/min otherwise.
     * Argon flow rate were controlled at 45 c.c./min, much lower than other samples.
     LT. Less Than

3.2 X-ray Diffraction Measurements

3.2.1 Introduction

X-ray diffraction methods (XRD) were introduced to study the microstructure of materials over

80 years ago. Today, it is still a powerful tool for obtaining structural information at the

angstrom level for a variety of materials. The equipment is relatively easy to operate and the specimens examined can still be used for other purposes because the method is nondestructive. The powder x-ray diffraction method is the most useful of all x-ray diffraction methods because single crystals are not always available and other forms of samples can be measured by powder diffraction without special preparation. In this method, monochromatic x-rays are diffracted by samples in polycrystalline form [28].

Since the first success in studying the crystalline structure of carbon by x-ray diffraction in 1924[29], a tremendous amount of work has been done in this area. In this project, x-ray diffraction was mainly used to investigate the average size of the graphene sheets in the carbons and the stacking properties of these graphene sheets.

3.2.1.1 Using x-ray diffraction to estimate the size of the graphene sheet

The Scherrer equations are used to determine the crystallite dimensions of various carbons. But as explained in Hang Shi's thesis[18], the dimension measured is not the particle size but rather the extent of small coherently scattering regions. In the Scherrer equations[28][30][31], the extent of the coherently scattering region normal to the graphene sheets (L_c) is estimated by,

$$L_c = 0.89\lambda / (B_c \cos \theta)$$

and the lateral extent of the sheets (L_a) is estimated by,

$$L_a = 1.84\lambda / (B_a \cos\theta)$$

where λ is the x-ray wavelength, θ is the Bragg angle, B_c and B_a are respectively the full width at half maximum of three dimensional and two dimensional Bragg peaks in radians. For disordered carbons, the 100 or 110 Bragg peak is used for the estimation of B_a and the 002 Bragg peak for B_c.

A typical x-ray pattern of our carbons (CL23IA) is shown in Fig. 3.2.1. Only very weak and broad 002, 100, 004 and 110 Bragg peaks are observed on a high level of background. This indicates that the carbons are highly disordered with a significant percentage of monolayer microstructures[32][33]. The single layers do not contribute to the intensity of the 002 Bragg peak, which originates from the coherent scattering by neighboring parallel layers, but add to the background at low angles. For this reason, L_c for our samples cannot be simply estimated by the Scherrer equations. Instead, we studied the stacking properties of the carbon samples by using the results of Drits and Tchoubar[32][33]. As discussed in Chapter 1.3.3, the single-layer fraction, which is the fraction of carbon atoms in randomly oriented single-layer microstructures, was the main stacking property we were interested in.

3.2.1.2 Using x-ray diffraction to study the stacking properties of the graphene sheets

The scattering intensity of the (002) Bragg peak, $I_{002}(q)$, for a powder sample of randomly positioned particles with randomly oriented microstructures of M graphite layers stacked parallel and spaced d_{002} apart, is calculated using the following equation 1[33],

$$I_{002}(q) = f^2(q)\frac{1}{q^2}\left[1 + 2\text{Re}\left[\sum_{n=1}^{M-1}\frac{M-n}{M}e^{inqd_{002}}\right]\right]$$
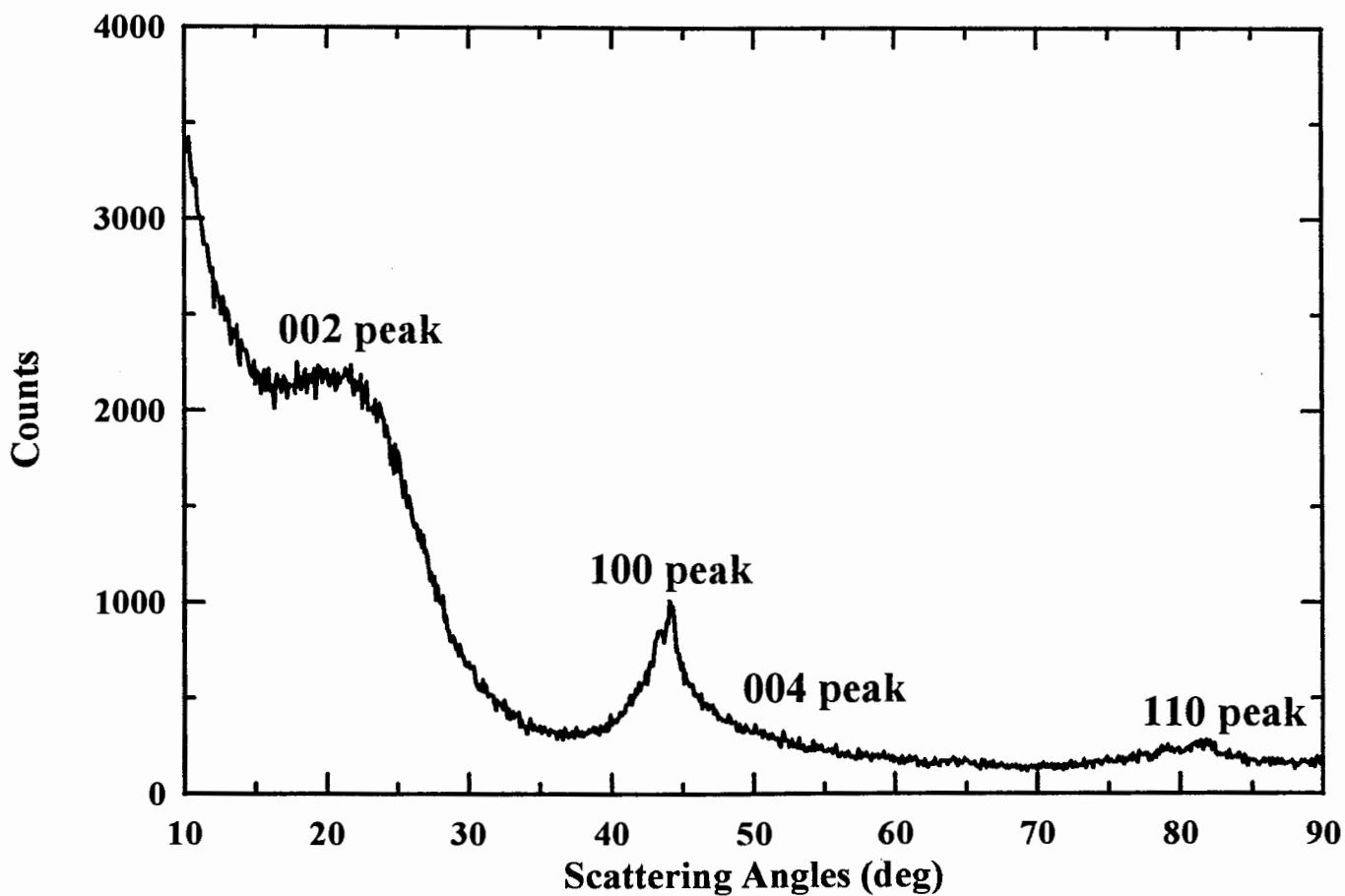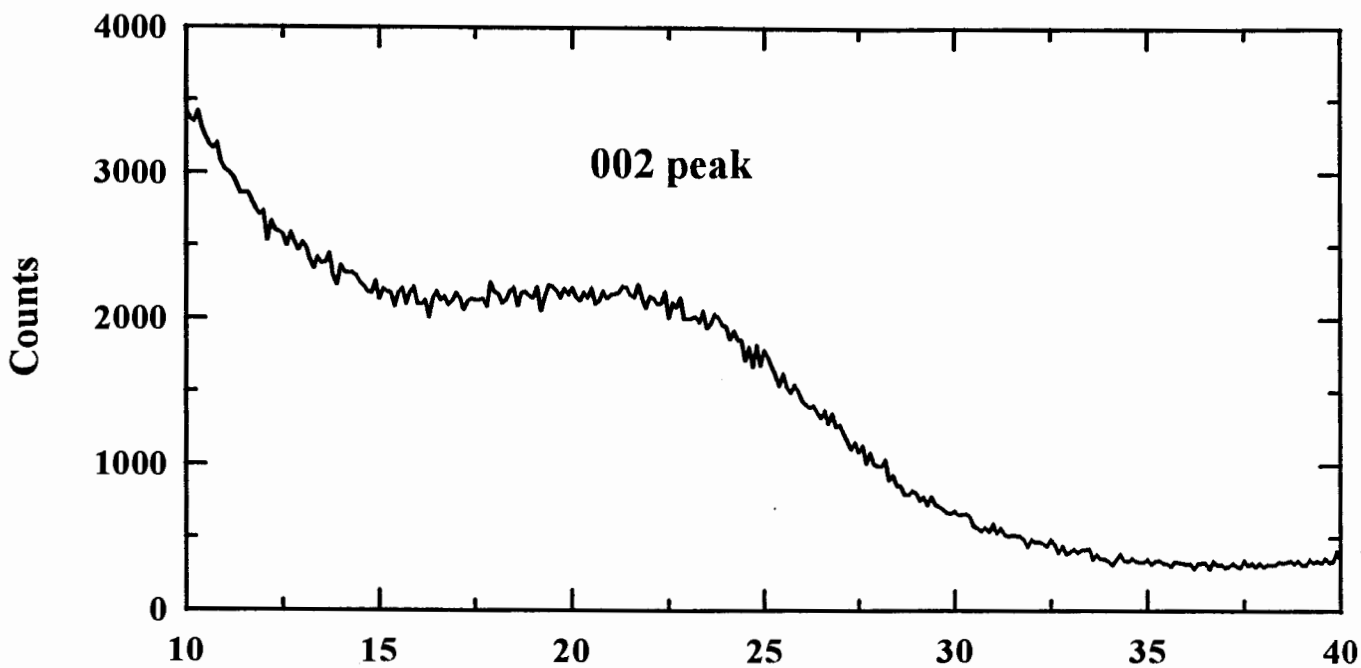
Fig. 3.2.1 Typical x-ray diffraction pattern of a sample prepared from epoxy novolac resin

where $q = 4\pi \sin\theta / \lambda$, is the wave vector, $f(q)$ is the atomic scattering factor of carbon and n is an integer summation index. The intensity per layer is $I(002)/M$. This expression is valid for scattering angles below about 37° where scattering from other Bragg peaks (for example (100)) is not observed. This equation further assumes that the graphite sheets have infinite lateral extent, which they do not have in experiment. Layers with finite lateral extent have slightly different low-angle scattering behavior due to their small size. For layers greater than 20Å in lateral size, equation 1 is accurate for scattering angles above about 5°.

We used equation 1 to calculate theoretical (002) Bragg peaks for different single-layer fractions. Fig 3.2.2 (a,b,c,d) shows the theoretical (002) Bragg peaks for samples with randomly oriented monolayer, bilayer and trilayer microstructures and for a sample with half of the atoms in monolayer and the rest in bilayer microstructures. Fig 3.2.3 shows the theoretical (002) Bragg peaks for a series of samples with a single layer fraction, f, ranging from 0.2 to 0.7, a bilayer fraction, 2/3(1-f), and a trilayer fraction, 1/3(1-f). As we will see, these profiles resemble those of experiment quite well.

3.2.1.3 Definition of R

Because of the difficulty in quantitatively fitting the x-ray diffraction patterns of these hard carbons, we defined an empirical parameter R to describe the stacking properties of the carbons. As shown in Fig. 3.2.4, R is the ratio of the total intensity to the background at the 002 Bragg peak position. In a sample with all single-layer microstructures, R reaches its lowest value of one (Fig. 3.2.2a). Fig. 3.2.5a and Fig. 3.2.5b show the (002) peaks and the overall x-ray profiles for
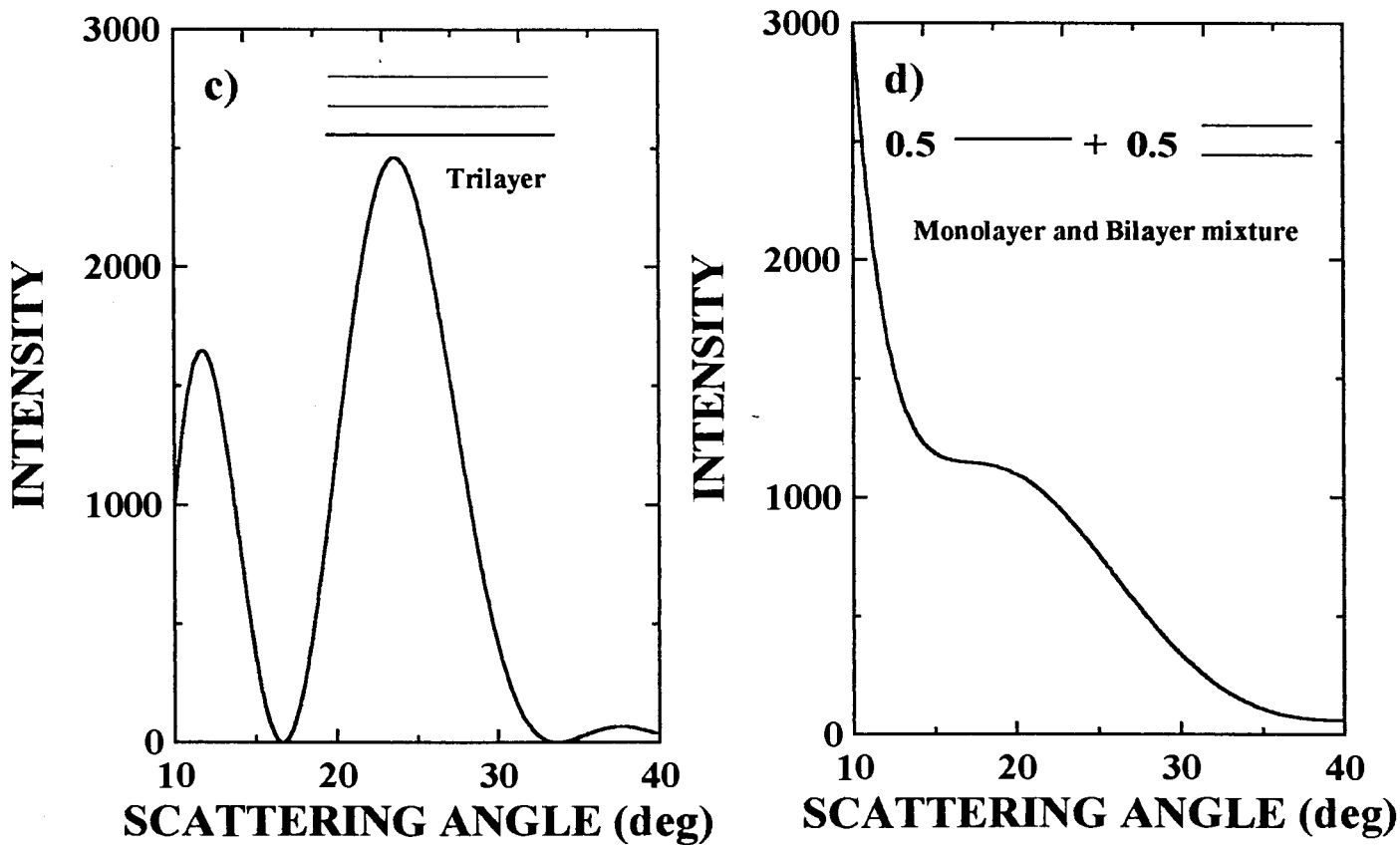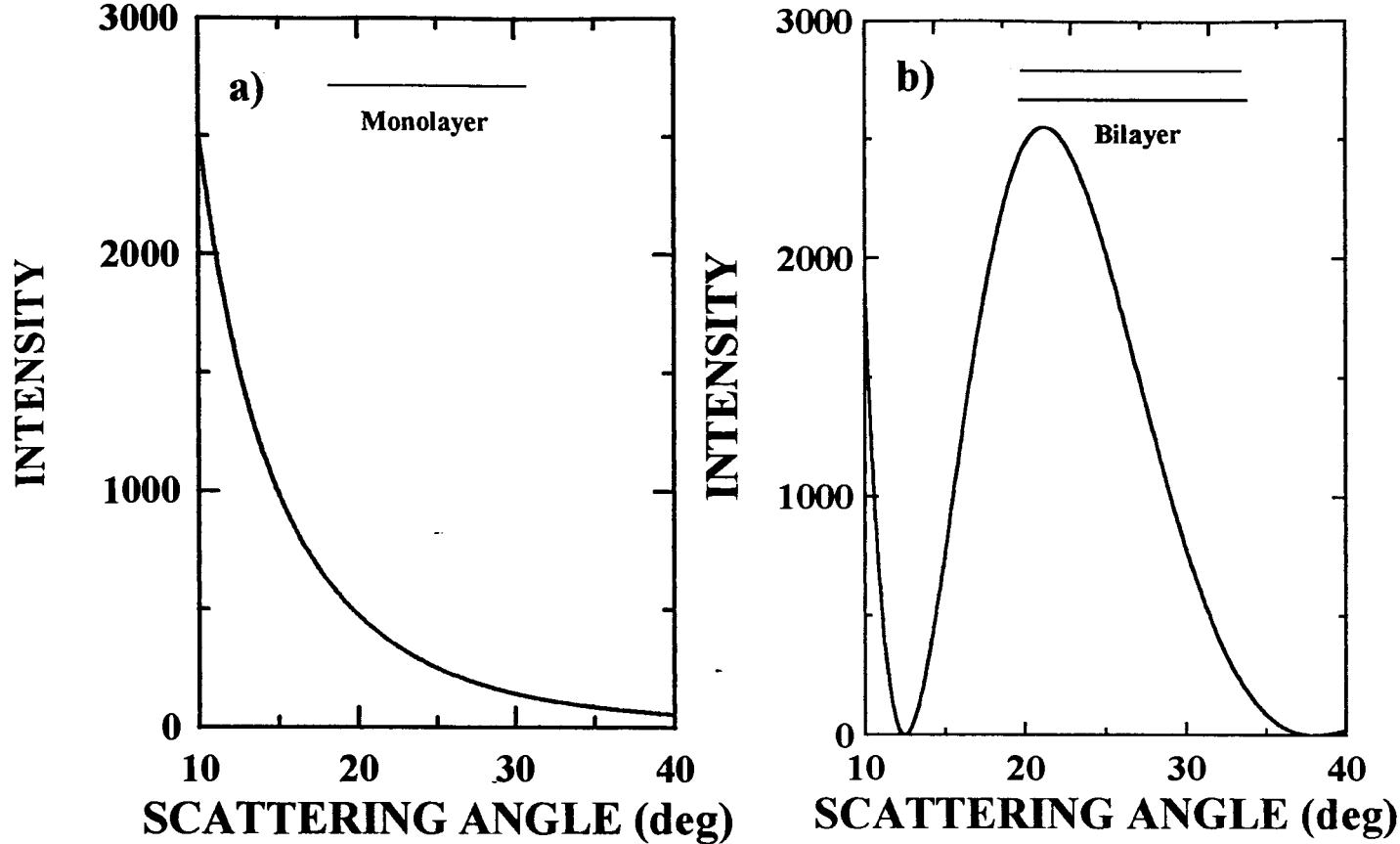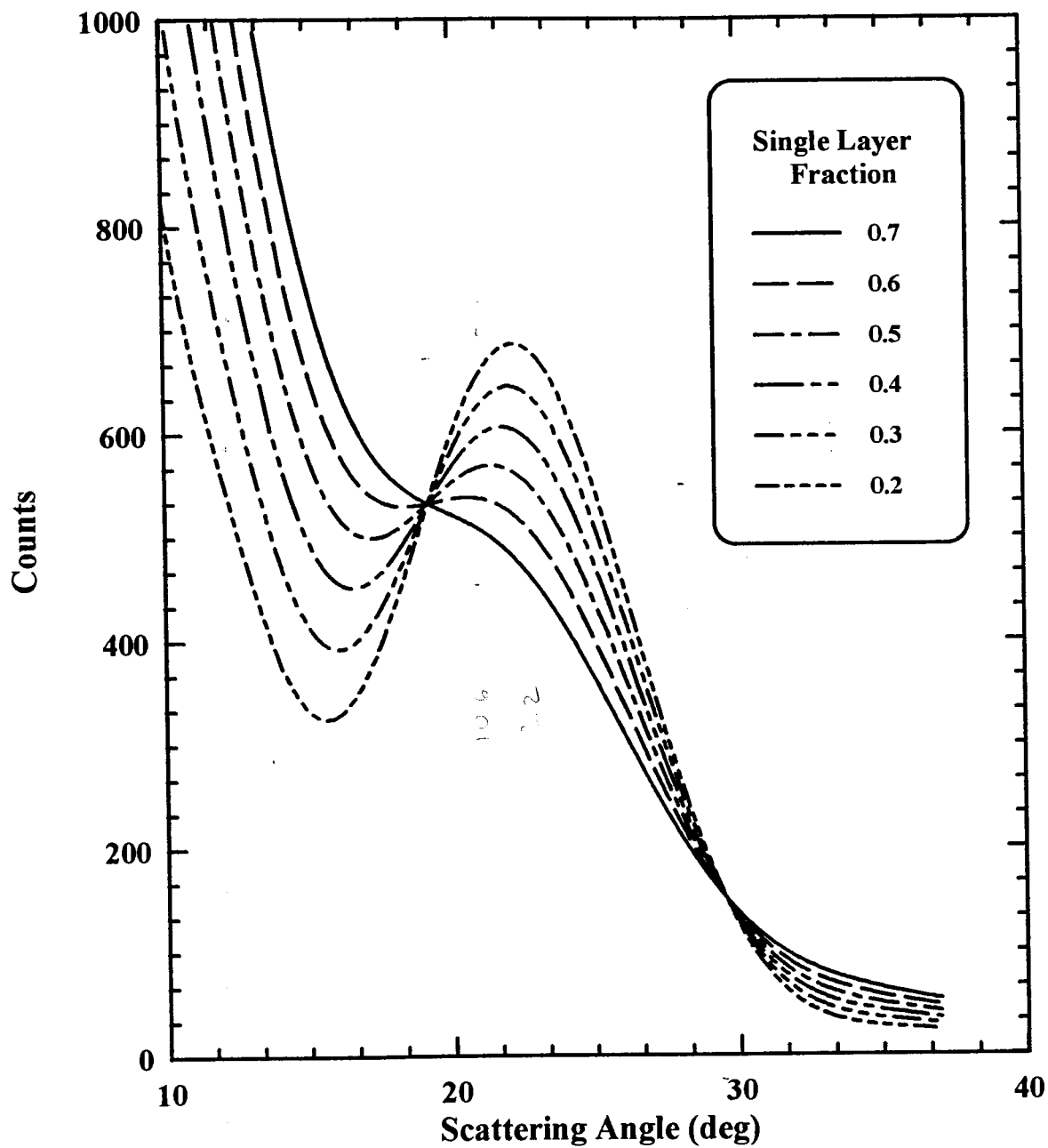
Fig. 3.2.2   002 Bragg peaks calculated for samples with different microstructures
——————— Carbon Sheet

Fig 3.2.3 Theoretical 002 Bragg peaks calculated using equation 1, for single-layer fraction f, bilayer fraction is 2/3(1-f) and trilayer fraction is 1/3(1-f)
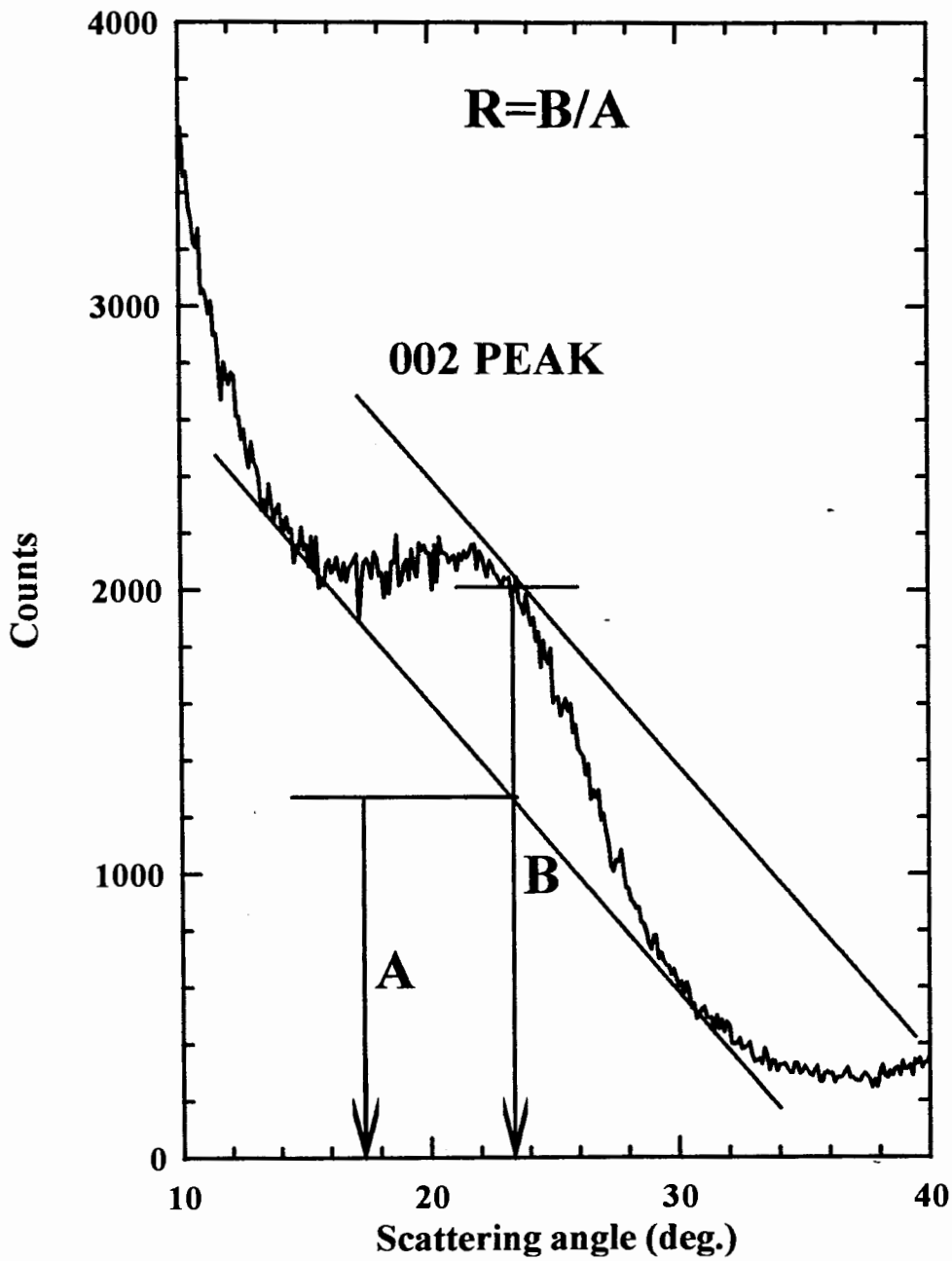
Fig. 3.2.4 Definition of R

a series of hard carbons made from hardened resins with a wide range of R values (CL12IA, CL17IC, CL38IB and CL21IA). The profiles were shifted 3000 counts sequentially for clarity.

3.2.1.4 The dependence of R on the single layer fraction of the sample

To estimate the dependence of R on the single layer fraction of the sample, the values of R for the theoretical patterns in Fig. 3.2.3, which exhibit the same trends as those of the experimental x-ray profiles in Fig. 3.2.5a, were calculated. These are plotted in Fig. 3.2.6 against their single layer fractions. Fig. 3.2.6 also shows R values for another set of theoretical (002) Bragg profiles where the bilayer and trilayer fractions were both taken to be 1/2(1-f) with f being the single layer fraction. Both curves in Fig. 3.2.6 show that R decreases as the single layer content of the sample increases and is fairly insensitive to how carbon is distributed in bilayers and trilayers. Thus, a measurement of R can be used to estimate the single-layer fraction of a carbon specimen using figure 3.2.6.

Figure 3.2.7 shows an attempt to quantitatively model the diffraction pattern of sample CL12IA using equation 1. The calculated pattern is for a sample with 50%, 30% and 20% of the carbon atoms in randomly oriented single layers, bilayers and trilayers respectively. The calculation agrees fairly well with the data and suggests that equation 1 could be used to extract the single-layer fraction of these carbon samples.
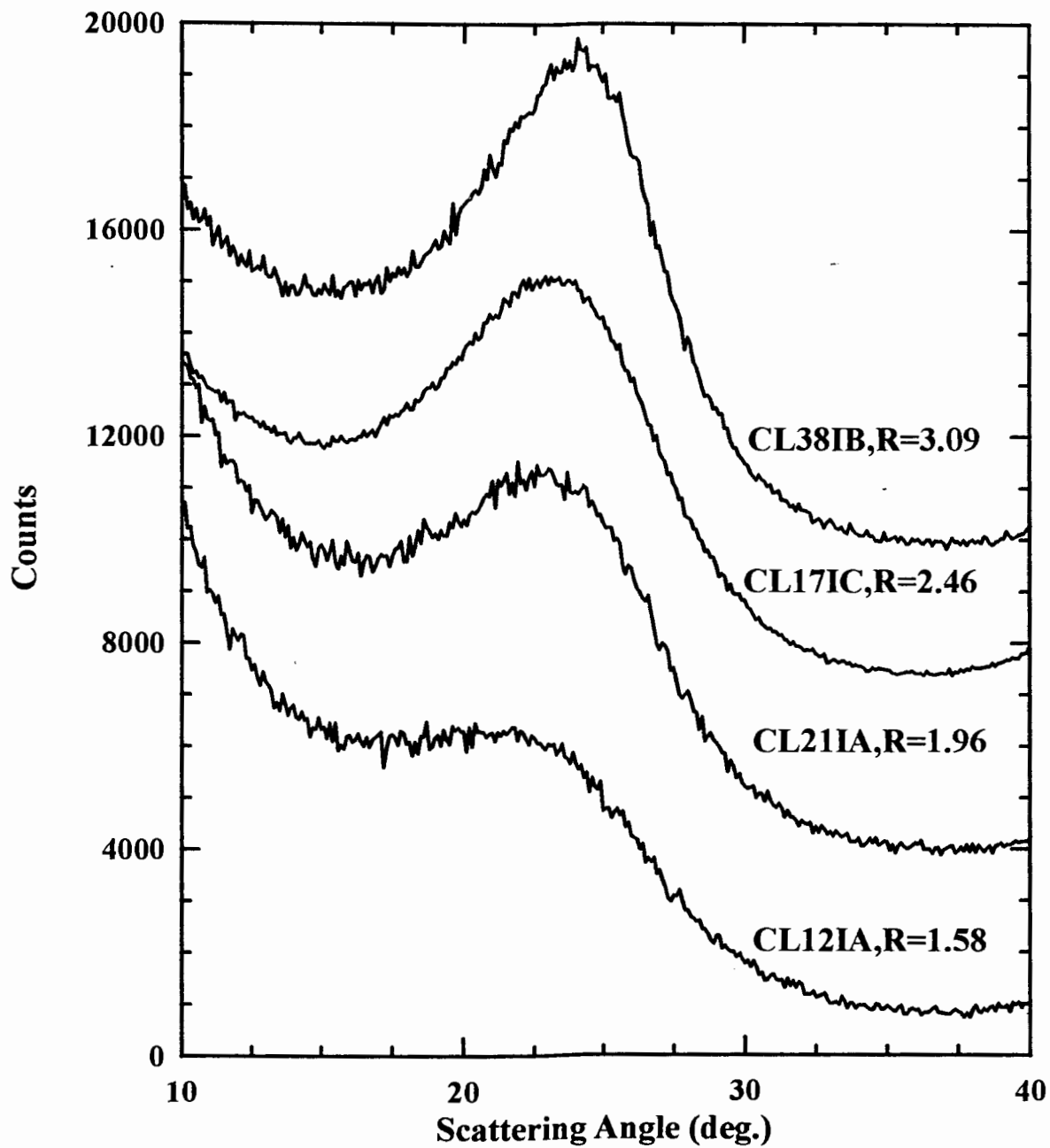
Fig. 3.2.5a 002 Bragg peaks of samples with typical values of R
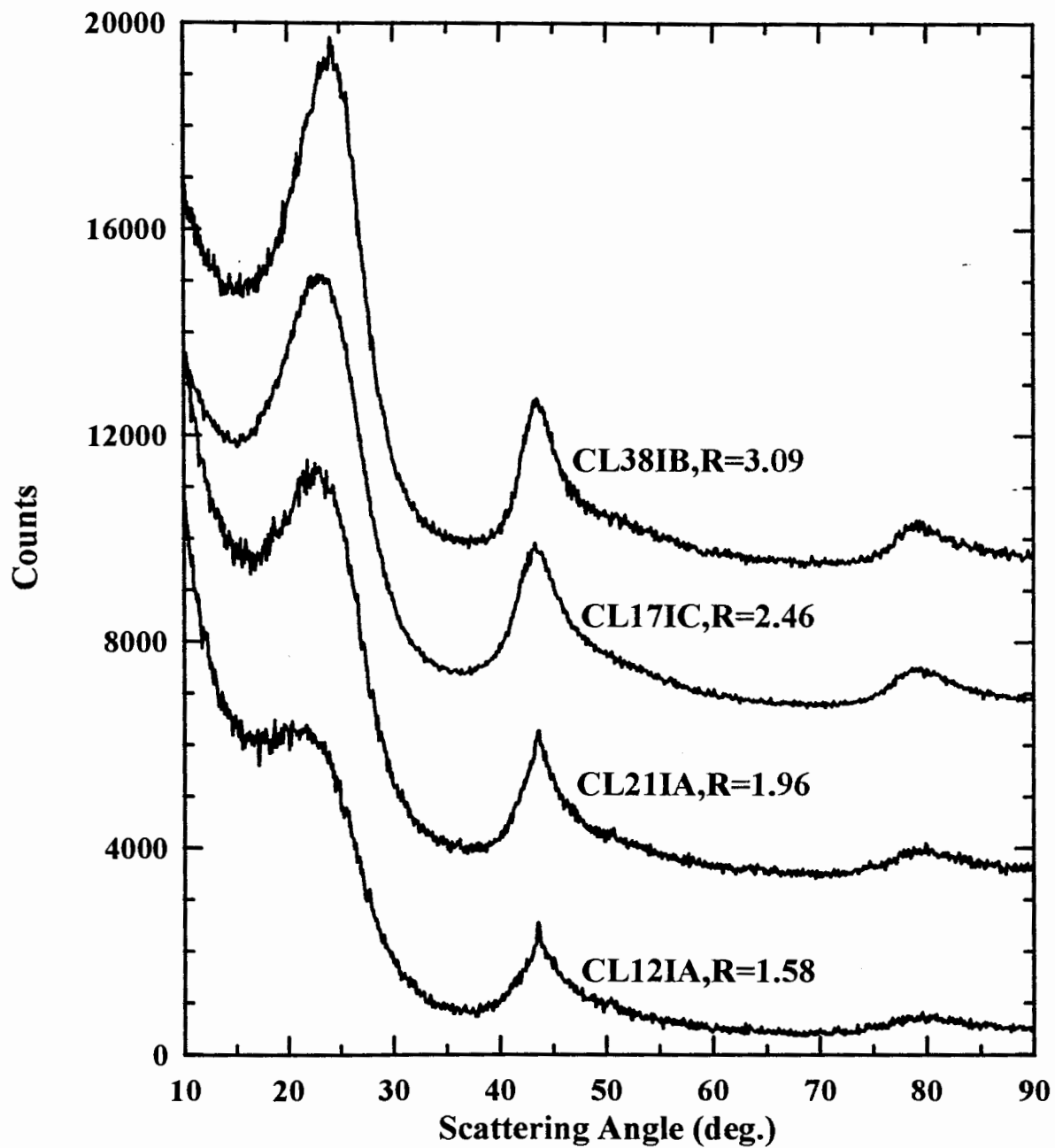
Fig. 3.2.5b X-ray profiles of samples with typical values of R
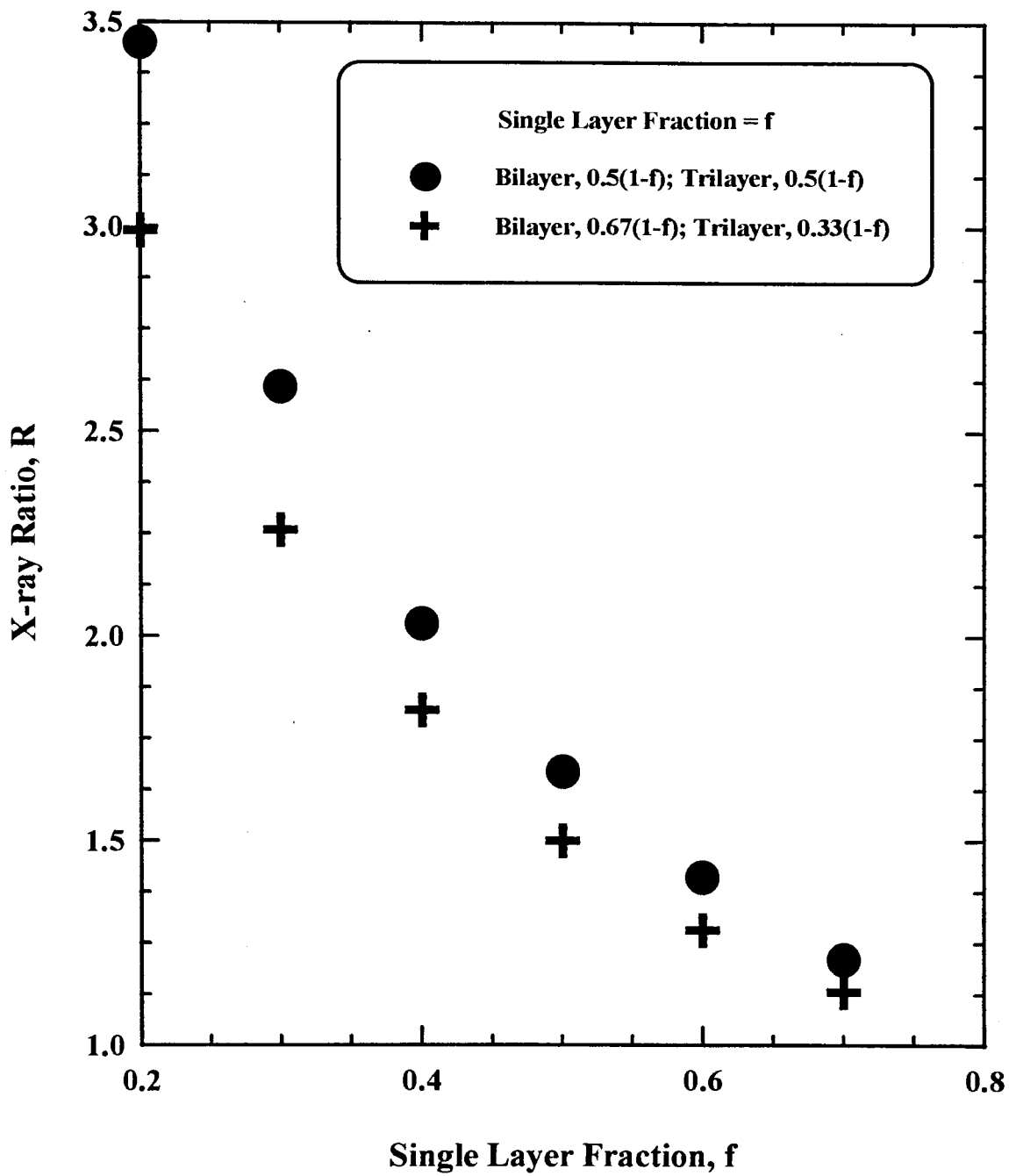
Fig. 3.2.6 X-ray ratio R versus single-layer fraction f
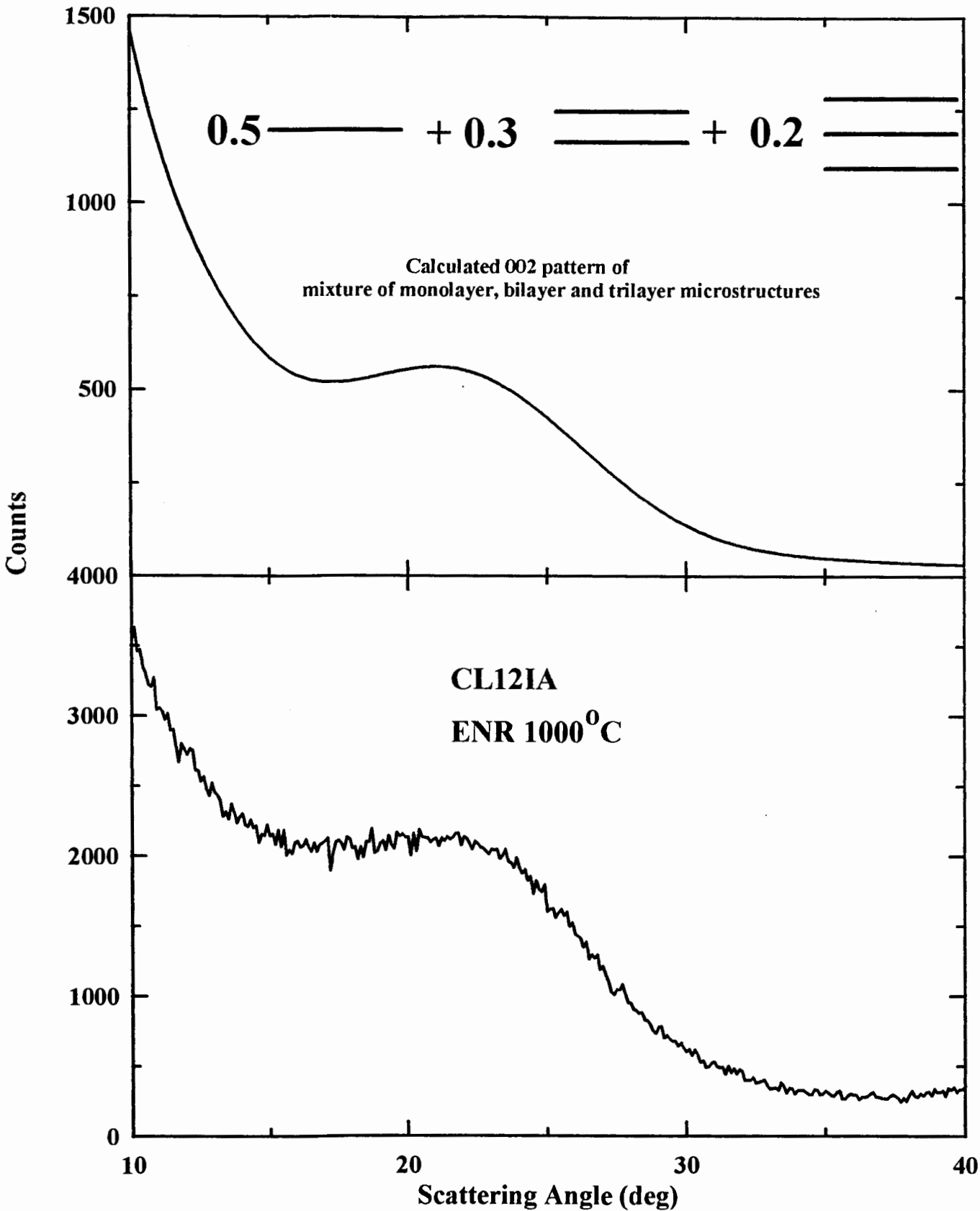
Fig 3.2.7 Comparison between a calculated and an experimenal 002 Bragg peak
———— carbon sheet

3.2.2 Equipment

X-ray diffraction measurements were made using a Siemens D5000 X-ray machine equipped with a copper target X-ray tube and a diffracted beam monochromator. The diffractometer operates in the Bragg-Brentano pseudofocusing geometry (see Fig. 3.2.8). The carbon powder to be tested was packed into a 2mm deep × 25mm long × 16mm wide 'well' inside a stainless steel holder to make a flat-plate specimen. The 0.5° incident slit used was selected so that none of the X-ray beam missed the sample in the angular range from 10° to 35° in scattering angle. The antiscatter slit was also 0.5° and the receiving slit was 0.6mm. The slit widths were fixed during the measurement and the same slits were used for all samples. This is important to ensure that the values of R, which were defined in figure 3.2.4, are meaningful.
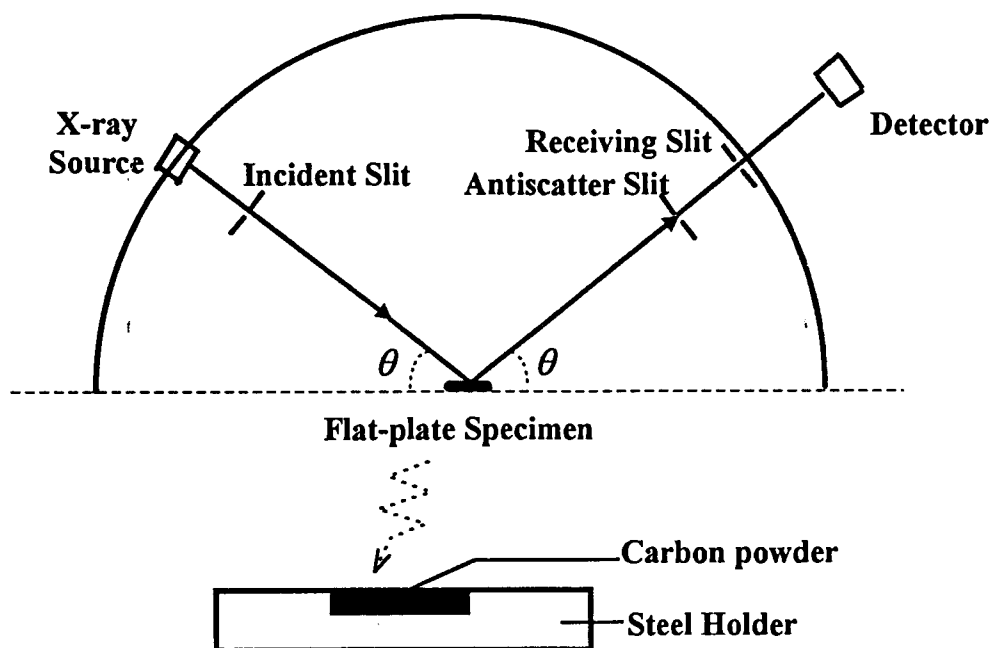
Fig. 3.2.8 Bragg - Brentano Pseudofocusing Geometry

3.2.3 Experimental results

We believe that carbons with the largest single layer fraction, hence low R, will have the largest capacity for lithium (see section1.3.3). To test this model, we made samples with different values of R. All the samples made are described in Table 3.2. Samples having the same series number were made from the same precursor. From table 3.2, it is obvious that the precursor is an important factor in determining the structure of the resulting carbons, which we do not fully understand yet. Three pyrolyzing parameters proved to be critical to the structure of the resulting carbons. They are the pyrolysis temperature, the heating rate and the morphology (powder or bulk) of the precursors.

Most of the samples were made at 1000°C. Fig. 3.2.9 shows the variation of R with heating rate for samples heated to 1000°C. For samples from bulk precursors (series 1 and 3) R increases as the heating rate decreases. But all three samples from powdered precursors which were heated at different rates (series 2) have approximately the same low R if we take the experimental error into account. How the argon flow rates influence R is not quite clear at this moment. The reasons why powdered precursors and high heating rates favor small R in the resulting carbon are as follows:

a) Large sample particles generate a higher partial vapor pressure of volatile organic products which may be able to re-deposit in a process akin to chemical vapor deposition, which is known to make soft carbons with large values of R. When these products are generated deep within the

40
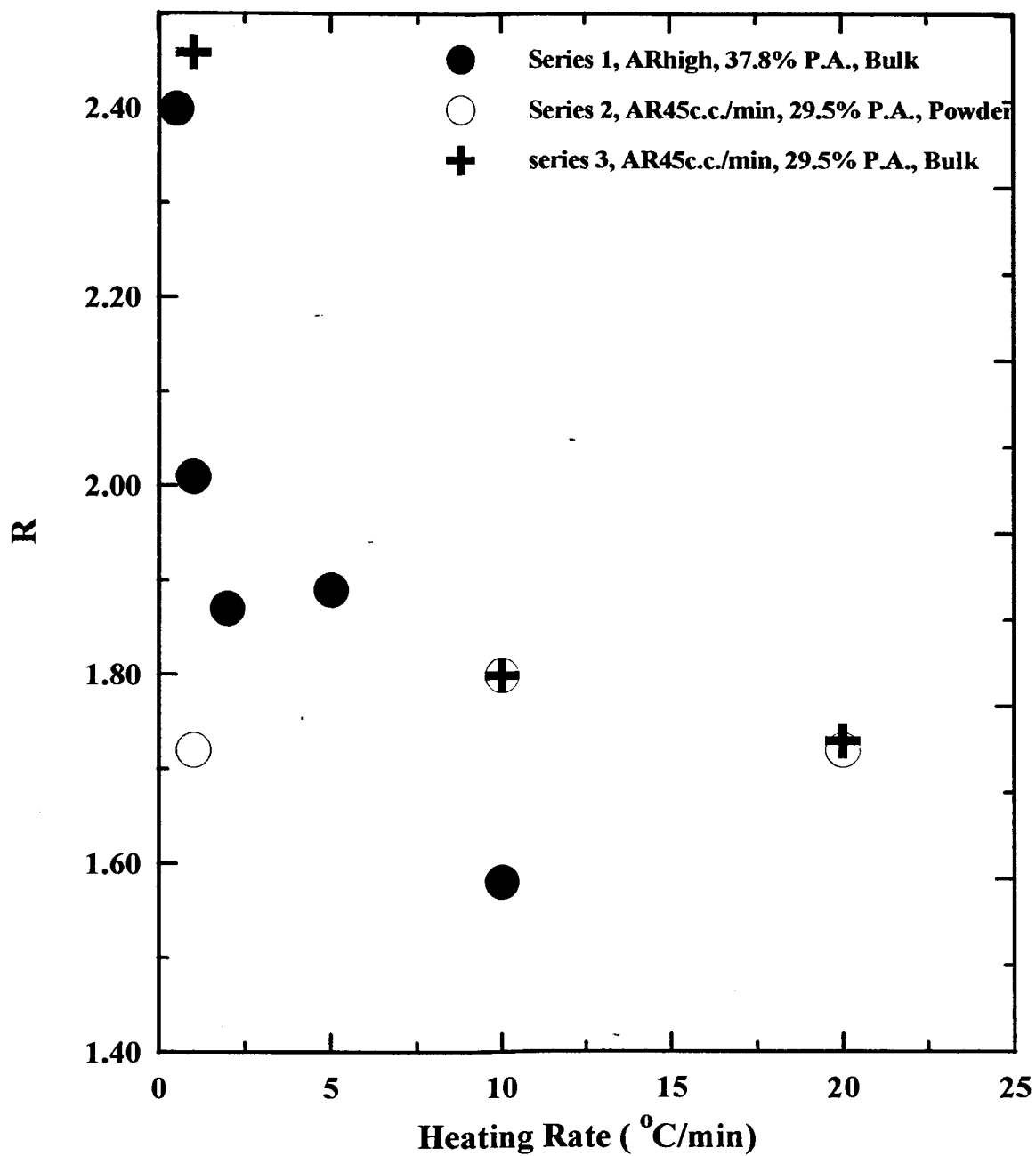
Fig. 3.2.9 R versus heating rate

bulk of a large "chunk", they must migrate through the chunk to reach the surface. We feel it is likely that substantial reattachment or redeposition of carbon atoms can occur during this migration, again tending to increase R. The grinding of precursors improves their ability to

Table 3.2 X- ray diffraction results, Values of R

SAMPLE ID	SERIES No.	$P.A.(%)	RAMP (°C/min)	TEMP (°C)	ISOTIME (min)	MORPH-OLOGY	La(Angstrom) (100)/(110)	R
CL38IB	N/A	14.8	#5,0.5,5	1100	120	BULK	43.5/40.0	3.09
CL52IB	1	37.8	#1,0.5,1	1000	60	BULK	36.2/32.5	2.40
CL14IA	1	37.8	1	1000	60	BULK	34.8/30.3	2.01
CL11IA	1	37.8	2	1000	60	BULK	37.0/35.9	1.86
CL13IA	1	37.8	5	1000	60	BULK	34.8/35.3	1.93
CL12IA	1	37.8	10	1000	60	BULK	34.8/31.6	1.58
CL45IA	4	22.8	20	700	60	BULK	31.2/21.9	1.57
CL46IA	4	22.8	20	800	60	BULK	32.8/31.8	1.59
CL46IB	4	22.8	20	900	60	BULK	32.8/NA	1.57
CL45IB	4	22.8	20	1000	60	BULK	35.6/30.8	1.75
*CL75IA	2	29.5	1	1000	60	POWDER	34.8/NA	1.72
*CL77IA	2	29.5	10	1000	60	POWDER	37.0/NA	1.80
*CL76IA	2	29.5	20	1000	60	POWDER	32.2/NA	1.72
*CL75IB	3	29.5	1	1000	60	BULK	36.2/NA	2.46
*CL77IB	3	29.5	10	1000	60	BULK	34.8/NA	1.80
*CL76IB	3	29.5	20	1000	60	BULK	34.8/NA	1.73
CL78IA		29.5	10	1000	60	BULK	34.8/NA	1.81
CL74IA		29.5	20	1000	60	BULK	35.6/NA	1.68

Note: $ Phthalic Anhydride.
   # Heating rate was 0.5°C/min from 300°C to 600°C and 1 or 5°C/min otherwise as indicated.
   * Argon flow rate were controlled at 45 c.c./min, much lower than other samples.
   LT. Less Than

release these organic decomposition products from the interior, thus preventing this type of redeposition.

b) According to Fitzer's work[13], degradation reactions proceed in a matter of seconds and less, while synthesis reactions to form aromatic macromolecules take the order of hours to finish. The reaction rate of cross-linking reactions is intermediate between the those two. All these reactions take place above around 350°C. Therefore, rapid heating leads primarily to the formation of small fragments representing a cracking gas and also to a disordered solid residue. Slow heating leads to synthesis reactions producing residues with more ordered carbon atoms. At high heating rates, such as 20°C/min, the samples in Table 3.2 from powdered and bulk precursors actually gave the same R under the same argon flow.

Some samples were heated to temperatures of 700°C, 800°C and 900°C. The purpose was to test our proposal[19] that the high capacities of the low temperature (<1000°C) carbons are caused by the high hydrogen contents of the materials. The heating rate used was 20°C/min and they were all made from bulk precursors. The resulting values of R were all low, but as we'll see later, they had very different electrochemical behavior from that of low-R carbons made at 1000°C.

Chapter 4   Electrochemical Tests

The carbons were used as electrode materials for rechargeable lithium batteries. Carbons with a wide range of R were used to test the dependence of the capacities for lithium on the single-layer fraction of the carbons.

4.1 Introduction

To determine the intercalation capacity of the carbons for lithium, we first need to relate the capacity to an experimental parameter that we can measure. In an electrochemical cell, when one Li^+ intercalates into the carbon through the electrolyte, one electron also moves to the carbon through external circuit. Therefore, the specific capacity is defined by the maximum amount of charge reversibly transferred between the electrodes per unit mass of the carbon material used in the electrode.

Consider a cell with carbon (host) as the cathode and Li metal as the anode (see fig. 1.1.2). The voltage of an intercalation cell is proportional to the chemical potential of the guest atom in the host material[34]. Suppose the chemical potential of lithium atoms in the host and in lithium metal are μ_c and μ_c^o respectively. Then the cell voltage, V, is calculated by: $-eV = \mu_c - \mu_c^o$
Thermodynamics requires that μ_c increase with the concentration of guest ion, so V decreases as ions are added to positive electrode (carbon). Thus measuring the cell voltage versus charge passed between the electrodes is equivalent to measuring the chemical potential as a function of x,

the Li concentration in the intercalated compound Li_xC_6. x is also used as a measure of the capacity of the host material. The relation between x and specific capacity, Q_r, is easily calculated to be, $Q = 372x \ mAh/g$. It is well-known that when x equals 1, Q_r is 372mAh/g for graphite. The electrochemical results presented here will be shown either in a Voltage - Capacity curve or a Voltage - x curve.

4.2 Cell Construction

4.2.1 Cell Design
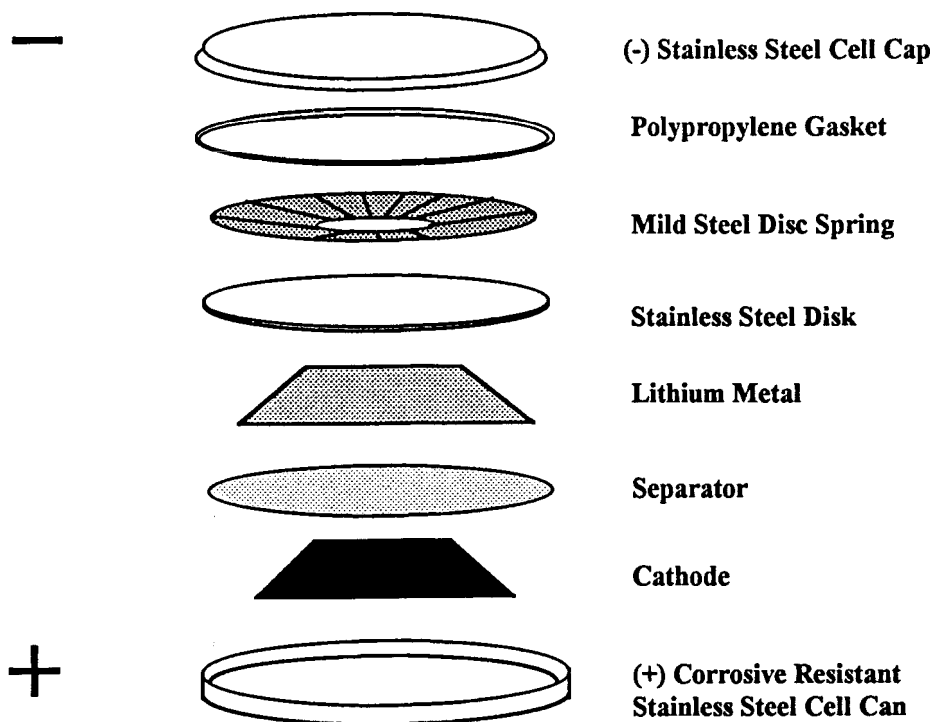
Fig 4.2.1 Exploded view of a typical lithium coin cell

Electrochemical test cells were constructed as shown in figure 4.2.1. 2325 coin cell hardware, equipped with a spacer plate (304 stainless steel) and a disc spring (mild steel) was used as the test vehicle. The disc spring was selected so that a pressure of about 15bar would be applied to each of the cell electrodes when the cell was crimped closed. The separator was Celgard 2502 microporous film which had been wetted with electrolyte. All cell construction and sealing were done in an Argon-filled glove box.

4.2.2 Anodes, Cathodes and Electrolyte

The anodes in the cells were 125µm thick, 1.2cm x 1.2cm square lithium foil sheets.

Cathodes were made from the carbon powder, super S carbon black (5% by weight) and polyvinylidene fluoride (PVDF) binder, uniformly coated on copper foil. Super S was used to improve the electrical contact between carbon particles[35]. The carbon sample and the carbon black were added to a solution of 9.4% PVDF in N-methylpyrollidinone (NMP) such that 5% of the final electrode mass would be PVDF. Excess NMP was then added until the slurry reached a smooth syrupy viscosity. The slurry was then spread on Cu foil using a spreader and the NMP evaporated at about 90°C in air. Once the electrode stock was dried, it was compressed between flat plates at about 25 bar pressure and cut into 1.2cm x 1.2cm squares. These electrodes were then weighed and the weight of the foil, the PVDF and the carbon black were subtracted to obtain the active electrode mass. Typical electrodes were 100µm thick and had an active mass of 15mg.

Due to the high reactivity of lithium metal and lithiated carbon with water, we used a nonaqueous electrolyte made of 1M $LiPF_6$ (Hashimoto) dissolved in a 30/70 volume percent mixture of ethylene carbonate (EC) and diethyl carbonate (DEC).

4.3 Cell Testing

4.3.1 Equipment

After construction, the cells were removed from the glove box and tested using computer-controlled constant-current cyclers with currents stable to ±1% (see Fig. 4.3.1). The cells were placed in thermostats at 30.0 ± 0.1°C during all tests. Currents were adjusted to be 7.4 mA/g, 18.5 mA/g or 37 mA/g of active material, depending on the desired test.
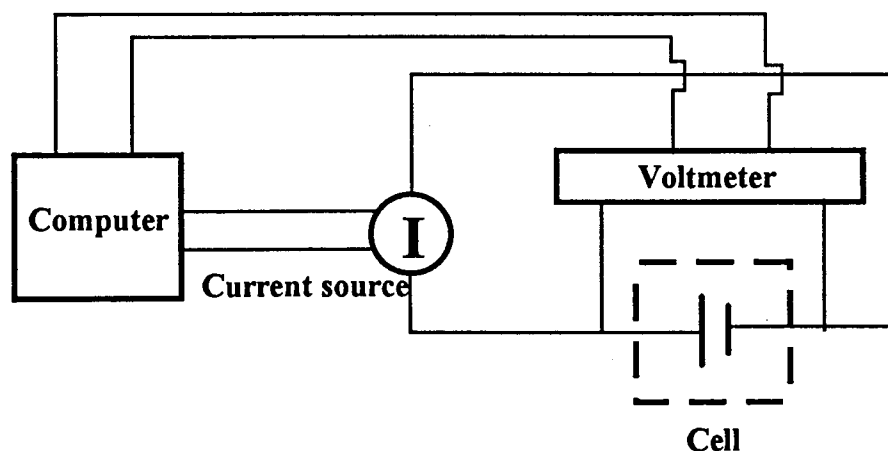

Fig. 4.3.1 Schematic of charger circuit

4.3.2 Testing Method

Much of the discharge capacity of these carbons is very close to the potential of lithium metal, which requires a special testing method to determine the full reversible capacity. A typical discharge - charge cycle of a cell is shown in Fig. 4.3.2. The x-axis of the curve is proportional to time; we simply multiply the time by the constant current used and divide by the active mass of the carbon electrode to get mAh/g as the unit for x-axis. We ignore the change of sign in the x-axis of the curve at the switch point. Most of our results are reported this way.

We discharged cells using a constant current for a fixed time chosen so that the cell voltage would fall below zero volts (versus Li) and so that lithium plating on the carbon would eventually occur. The plating does not occur immediately after the cell voltage goes below zero volts because of the overvoltage caused by the finite constant current used. However, plating does begin shortly thereafter (usually around -0.02V) and is characterized by a region where the voltage of the cell rises slightly once the plating is initiated , followed by a constant or near constant voltage region. The onset of lithium plating is clearly and easily determined as we will show below. The plating of lithium on the carbon is continued for a few hours and then the current is reversed. First the lithium metal is stripped, and then the inserted lithium is removed from the carbon. The two processes are easily distinguished provided the charge rates are small (less than 37mA/g).

We calculate the reversible capacity as the average of the capacities excluding lithium plating and stripping of the second discharge and charge cycle of the cell. The first discharge is not used because irreversible processes[36] occur on the first discharge. It is advisable to minimize these irreversible processes as much as possible in materials for practical cells.
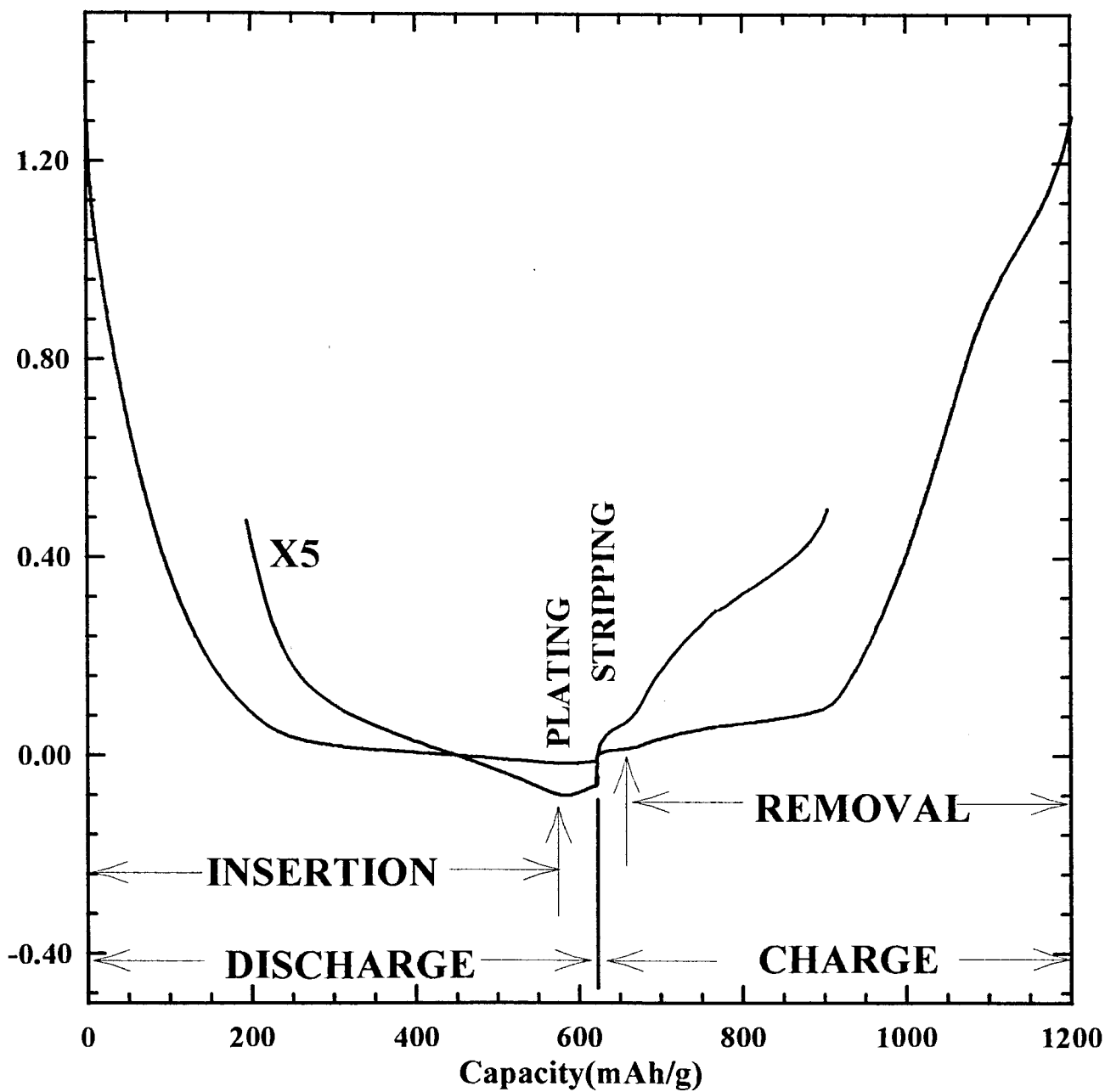
Fig. 4.3.2 A discharge - charge cycle showing how lithium plating and stripping can be distinguished from the insertion reaction

4.3.3 Testing Results

Information regarding the cells made is listed in Table 4.1.

4.3.3.1 Specific capacity and single layer fraction

The chemical composition of pyrolyzed organic compounds and the lateral extent of the graphene sheets are known to depend on pyrolysis temperatures. To minimize these effects and to explore the changes on the insertion of lithium induced by changes in the single-layer fraction, we plotted the reversible capacity of samples made at 1000°C against R values in Fig. 4.3.3. There are also two samples made at 900°C and 1100°C respectively in Fig. 4.3.3 to enlarge the range of R. Table 4.1 shows that they both have similar L_a and H/C atomic ratio to those of the samples made at 1000°C. Fig 4.3.3 shows a clear trend as we predicted earlier in chapter 1; that is, samples with smaller R and therefore having more single-layer microstructures give larger specific capacity. An extrapolation of the data in Fig 4.3.3 to R=1 (all single layers), gives a reversible specific capacity near 700mAh/g, which is about 2 lithium atoms per 6 carbons as hypothesized in chapter 1.

Fig. 4.3.4 is the voltage versus capacity curve for four samples from Fig. 4.3.3 with representative values of R. The curves of R=3.09, 2.46 and 2.05 in the lower graph were shifted up by 0.6, 0.4 and 0.2V for clarity. The capacity of the low-voltage plateau (~0 volt) increases dramatically as R decreases and the single-layer fraction of the sample increases. Lithium adsorbed on the surfaces of single layers should probably be quite weakly bound. This implies that the voltage of a lithium /(single-layer carbon) cell should be very near zero volts, as observed for the long plateau in figure
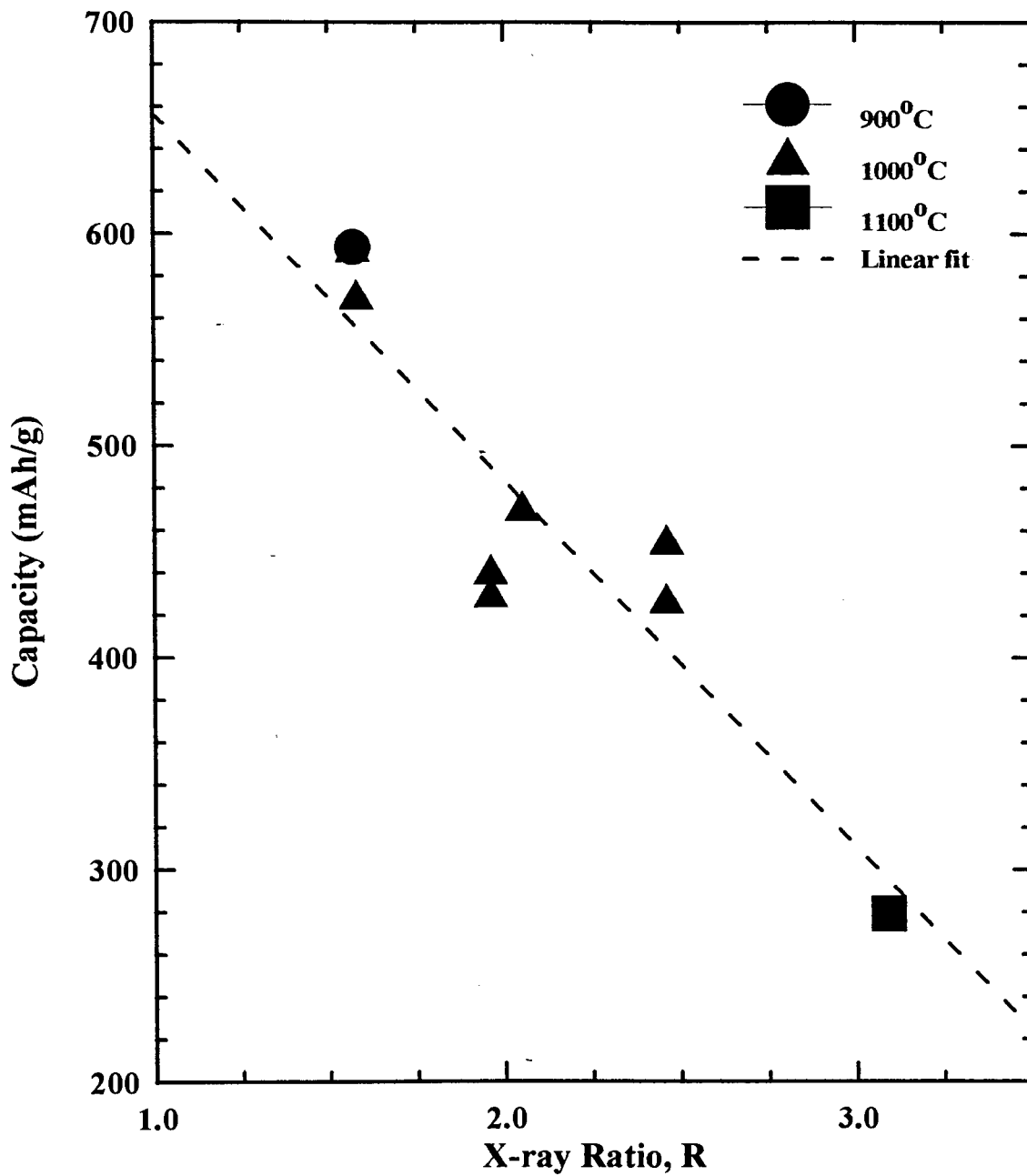
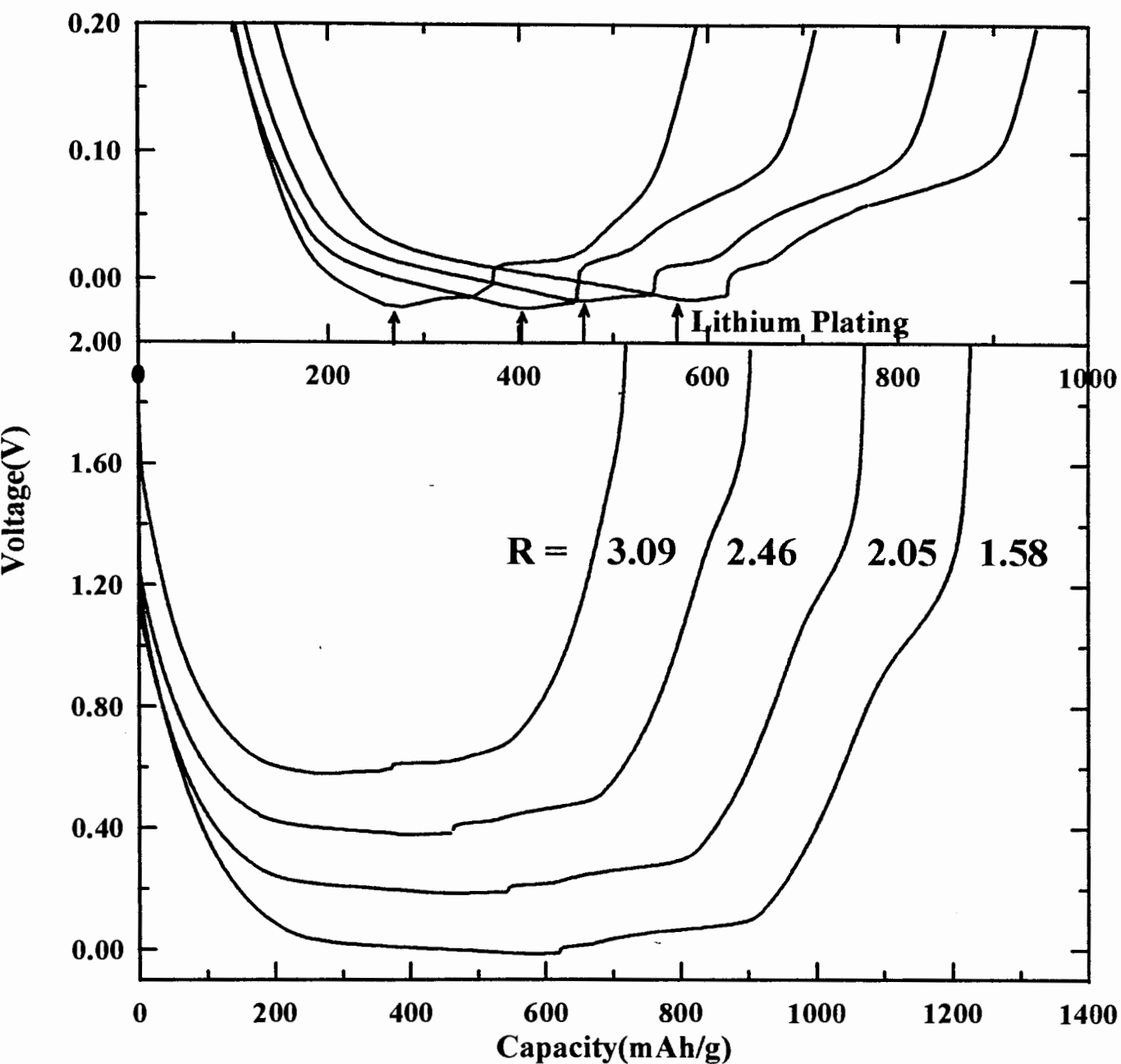**Fig. 4.3.3 Reversible specific capacity of epoxy samples versus R**

Fig. 4.3.4 Showing how the low voltage plateau changes with R

4.3.4, which grows with single-layer content. This again supports our hypothesis of adsorption of lithium on both sides of these carbons. The steeply sloping portion of the voltage profiles in Fig. 4.3.2 and Fig. 4.3.4 probably arises from the insertion of lithium between carbon layers which are stacked in a roughly parallel fashion.

4.3.3.2 Specific capacity and H/C atomic ratio

As shown in Table 4.1, we also studied the insertion of lithium into samples pyrolyzed below 1000°C. The hydrogen content of these samples decreases when the pyrolysis temperature increases. Fig. 4.3.5 shows the voltage versus capacity curves of samples made at 700°C, 800°C, 900°C and 1000°C. Although each of these samples has high reversible capacity around 600mAh/g, the voltage curves are very different. For the sample made at 700°C, the majority of the capacity shows high hysteresis; that is, the lithium is inserted near zero volts (versus lithium metal) and removed near one volt. As the samples were heated above 700°C, the H/C atomic ratios and the capacities with high hysteresis decreased simultaneously. But the total reversible capacities did not decease correspondingly because the low plateau with little hysteresis grew as the H/C ratios were decreased. Samples from a variety of precursors were made at temperatures from 550°C to 1000°C by Zheng et. al[19] and showed that the capacity with high hysteresis is proportional to the H content of the samples.

Several mechanisms were proposed to explain the high capacity exhibited by carbonaceous materials made at relatively low temperatures. A good summary can be found in either Zheng's[19]
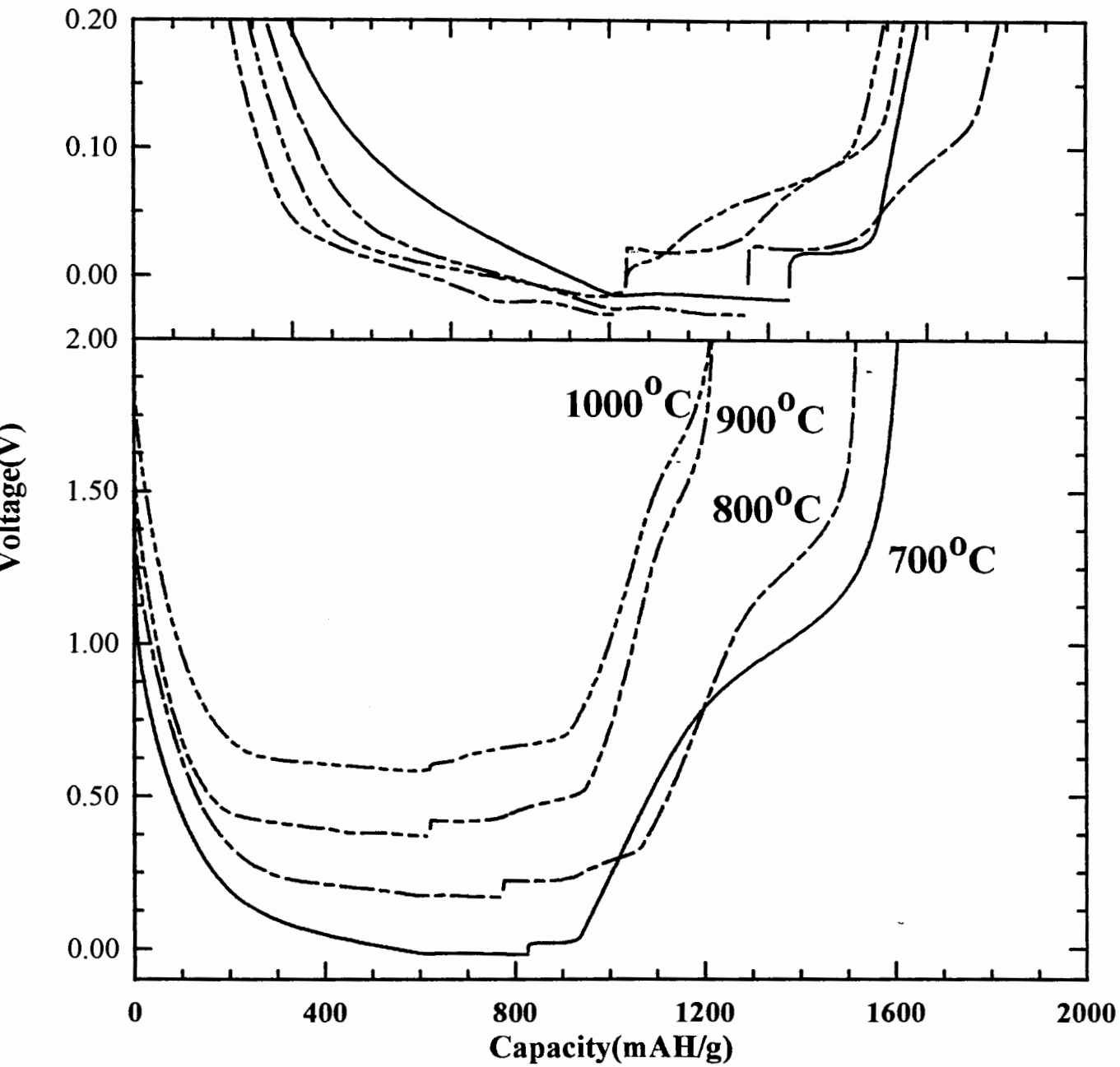
Fig. 4.3.5 Voltage curves of samples pyrolyzed at different temperatures

or Dahn's paper[37]. Sato et al[38] proposed that lithium atoms can occupy nearest neighbor sites between graphite sheets in their high capacity material made from polyparaphenylene heated to 700°C. Based on NMR (Nuclear Magnetic Resonance) results, Mabuchi et al [39] proposed that lithium can be inserted in the nanopores, as small clusters of metallic lithium, within their high capacity material made from coal tar pitch heated to 700°C. These two mechanisms do not predict a large hysteresis, but the voltage curves in both papers showed a hysteresis of about one volt. Sato et al.'s proposal also failed in explaining why lithium cannot be inserted in near-neighbor sites in graphite itself. Zheng et al[19] included the data from both papers, along with data of their own samples, in the capacity versus H/C atomic ratio curve and showed a striking correlation between the capacity for lithium of hydrogen-containing carbons and their hydrogen content.

According to Enoki's work on hydrogen-alkali-metal-graphite ternary intercalation compounds[40], alkali metals can transfer charge to hydrogen. Enoki et al. first intercalated graphite with the alkali metal and then reacted it with hydrogen gas. For the samples we made at a temperature near 700°C, there were already hydrogen atoms bonded to carbon atoms at the edge of small graphene sheets (see Fig. 4.3.6). If lithium can still transfer part of its charge to H when intercalating into these hydrogen-containing carbons, the high capacity for lithium should be proportional to the H content of the materials. Because inserting and removing the lithium atoms involves the establishing and breaking of bonds as shown in Fig. 4.3.6, hysteresis is introduced into the charging-discharging process[41].
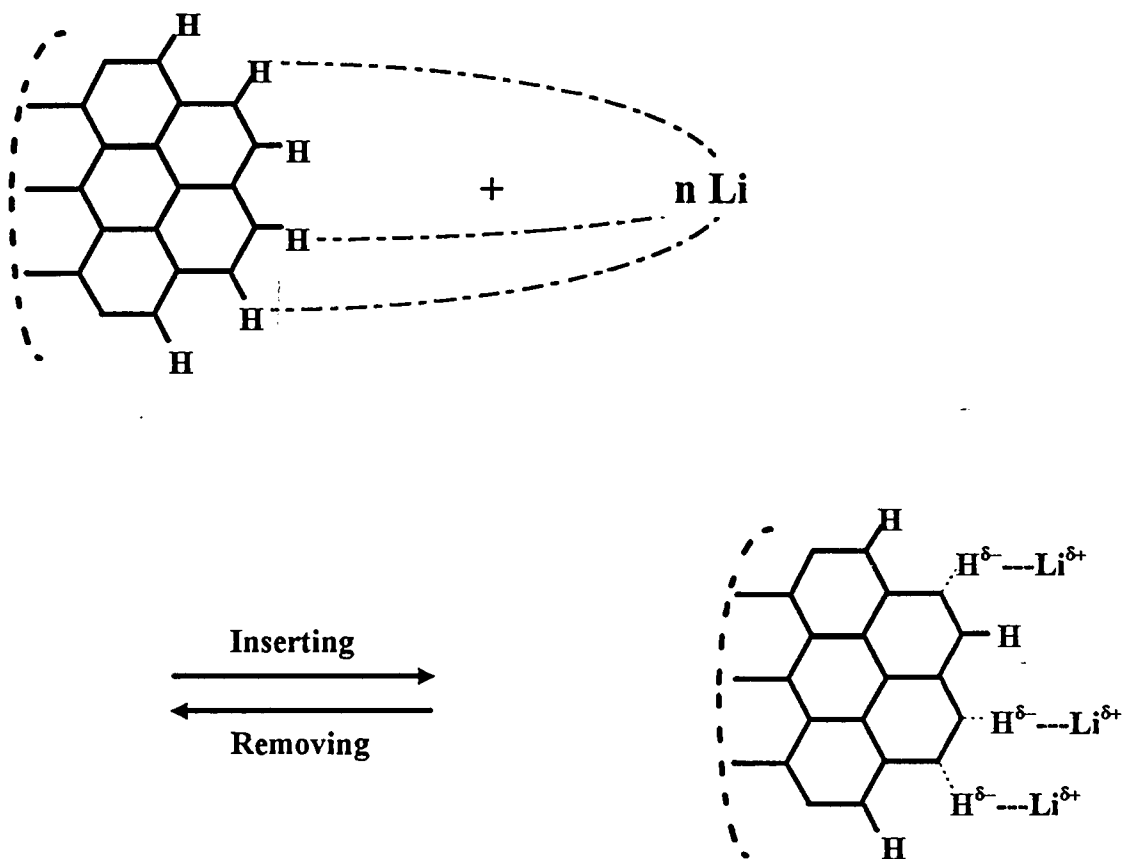
Fig. 4.3.6 Proposed mechanism of lithium insertion into H containing carbons

Table 4.1   Cell information sheet

CELL ID	CATHODE ID	$P.A. (%)	TEMP. (°C)	HEATING RATE (°C/min)	ISOTIME (hr)	H/C ATOMIC RATIO	La(Angstrom) (100)/(110)	X-RAY (R)	CAPACITY (mAh/g)	BET (m²/g)
RR1.940614.601	CL17IA	0	1000	1	1	0.033	34.8/32.7	2.05	471.71	148
RR1.940614.603	CL17IC	14.8	1000	1	1	0.087	37.1/34.2	2.46	455.82	16
RR1.940614.604	CL17IC	14.8	1000	1	1	0.087	37.1/34.2	2.46	428.18	16
RR1.940621.601	CL12IA	37.8	1000	10	1	0.03	34.8/31.6	1.58	571.37	205
RR1.940721.602	CL38IB	14.8	1100	#5, 0.5, 5	2	0.025	43.5/40.0	3.09	279.13	4.26
RR1.940722.601	CL21IA	14.8	1000	1	1	NA	32.8/36.0	1.96	430.98	17.9
RR1.940722.602	CL21IA	14.8	1000	1	1	NA	32.8/36.0	1.96	441.72	17.9
RR1.940728.602	CL45IA	22.8	700	20	1	0.166	31.2/21.9	1.57	651.51	
RR1.940803.601	CL46IA	22.8	800	20	1	0.111	32.8/31.8	1.59	609.72	
RR1.940809.601	CL46IB	22.8	900	20	1	0.067	32.8/NA	1.57	593.96	

Note: $ Phthalic Anhydride.
   # Heating rate was 0.5°C/min from 300°C to 600°C and 5°C/min otherwise.
   * Argon flow rate were controlled at 45 c.c./min, much lower than other samples.
   LT. Less Than

Chapter 5   Summary and Suggestions for Future Work

5.1   Mechanisms of Lithium Intercalation into Different Carbonaceous Materials

Fig. 5.1.1 shows the voltage curves of cells made from graphite, hard carbon made by pyrolyzing epoxy resin at 1000°C, and high-hydrogen-content carbon made by pyrolyzing epoxy resin at 700°C. The difference in the profiles indicates that insertion of lithium atoms into these materials follow three different mechanisms.

5.1.1 Lithium Intercalation into Graphite

The intercalation of lithium in graphite has been well studied. I will give a brief review just for comparison purposes. Under ambient conditions, the maximum amount of lithium that can be intercalated into crystalline graphite is 1 lithium atom per 6 carbon atoms[42, 43]. In LiC_6 (see figure 1.3.2), the lithium atoms occupy next-nearest neighbor sites, separated by 4.35 Å, between each pair of carbon sheets. When the lithium is intercalated, it transfers most of its 2s electron to the carbon host and exists as a screened ion between the carbon sheets. The Coulomb repulsion between lithium ions forbids them to take the nearest-neighbor sites and metallic lithium co-exists with LiC_6 in any compound Li_xC_6 with $x>1$. Recent research[15] showed that samples with $x>1$
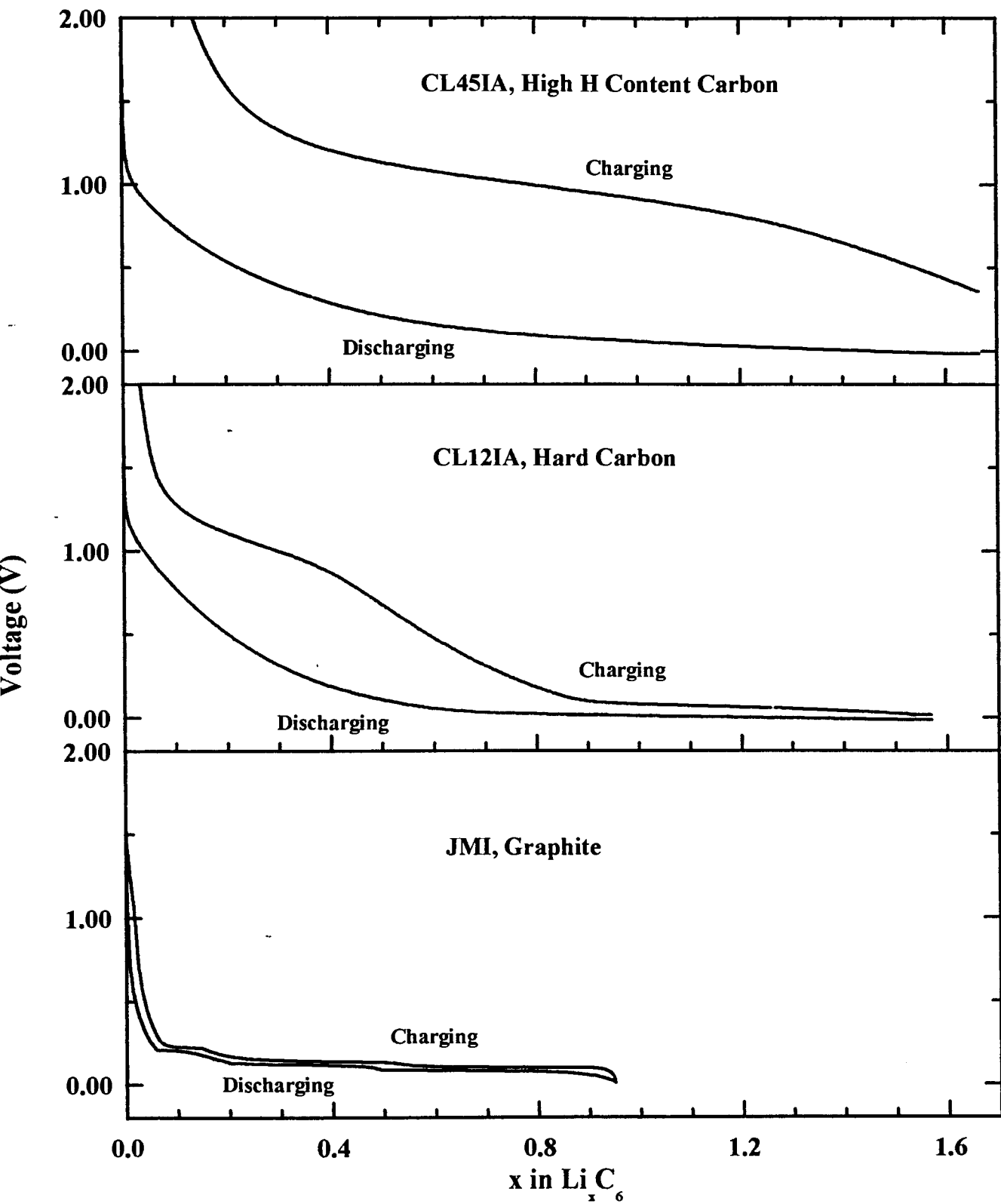
Fig. 5.1.1 Voltage curves of cells using different carbons as electrodes

could be made from graphite under extreme conditions (280°C and 50 kBar Li vapor pressure) by forcing the lithium to occupy nearest neighbor sites in the resulting Li_xC_6 compound.

5.1.2 Lithium Insertion into High Hydrogen Content Carbons

The high capacities of hydrogen-containing carbons are closely correlated to their hydrogen content[19]. Enoki et al[40] showed that charge transfer from alkalis to hydrogen in intercalated carbons is observed. Therefore, we believe that lithium atoms can bind in the vicinity of H atoms in these hydrogen-containing carbons. The inserted lithium atom can transfer part of its 2s electron (in a covalent bond) to a nearby hydrogen, resulting in a change to the carbon-hydrogen bond. The bond changes which occur while inserting and removing lithium might lead to hysteresis[41], which is a characteristic of the voltage profiles of cells made from hydrogen-containing carbons.

5.1.3 Lithium Insertion into Hard Carbons with Low Hydrogen Content

The main goal of this project was to substantiate the proposal we gave in chapter 1 that the high capacities of hard carbons are due to the adsorption of lithium on both sides of the single-layer graphene sheets in these materials. In chapter 3, we defined an empirical parameter R based on the shape of the 002 Bragg peak of the x-ray profile and found that it is inversely correlated with the single layer fraction of the material. We made materials with different values of R but containing graphene sheets of similar lateral extent. We used these materials as the electrodes in

rechargeable lithium batteries and tested their capacities for lithium. As shown in chapter 4, we found that the capacity increases as R decreases and the single-layer fraction of the material increases. Also as mentioned in chapter 4, an extrapolation of the capacity versus R curve to R=1 (all single-layer material) will lead to a capacity of about 700mAh/g, that is, about 2 lithium atoms per 6 carbon atoms. This also supports our proposal.

Ishikawa et al[44] suggest that the high capacities of hard carbons is due to the filling of nanopores with lithium. As shown in Fig. 1.3.3, it is easy to understand that hard carbons with a significant percentage of single layer microstructures must contain a fair number of nanopores. Hard carbons made from epoxy resins have been shown to be nanoporous using small-angle-x-ray scattering[45]. When the pores are small enough, (SAX shows they are in the order of 15Å in diameter) the adsorption of lithium on the pore surfaces will fill a large fraction of the pores. In either pore-filling or surface-adsorption models, we expect the lithium to be weakly bound with respect to lithium in lithium metal, consistent with the low-voltage plateau in the voltage profile.

5.2 Practical Considerations

Carbonaceous materials with high hydrogen content and relatively pure hard carbons with large single-layer fractions, made by pyrolyzing hardened novolac resins at different temperatures, have capacities almost twice as large as that of graphite. However, hysteresis is found in the voltage curves of cells using carbons with high H content as electrodes. The presence of large hysteresis makes these materials unsuitable for lithium-ion batteries because then cells have to be charged

near 4 volts to deliver about 3 volts during discharge. Voltage curves for fairly pure hard carbons with large single-layer fractions show little hysteresis and therefore these carbons are desirable for Li-ion cells.

5.3 Suggestions for Future Work

There is still a lot of theoretical and experimental work that should be done to fully understand the mechanisms of lithium insertion into these materials and to exploit the high capacity of these materials.

First of all, the microstructure of these materials should be examined quantitatively. Better models should be developed to fit the x-ray patterns of these materials. Small angle x-ray (SAX) measurements have been performed to study the nanoporosity of these materials[37]. Other techniques, like TEM, should also be used to confirm the results from SAX and to give new information on the microstructure of these materials.

Most importantly, inexpensive precursors other than epoxy novolac resin should also be tried to produce hard carbons with high single-layer fraction, and therefore to find the most economical materials of the highest quality for Li-ion industry. Other factors, such as cycling performance, should also tested.

In conclusion, hard carbons with a large fraction of carbon atoms in randomly oriented single-layer graphene sheets are very promising candidates for anodes of lithium-ion batteries. However, there is still a lot to be understood in this exciting area.

References

[1] M.S. Whittingham, *Science 192*, 1126, (1976).

[2] R.R. Haering, Editor, *Proceedings of the 4th International Meeting on Lithium Batteries,* Vancouver, B.C. (1988).

[3] For example, see 'Cellular Phone Recall May Cause Setback for Moli', *Toronto Globe and Mail,* August 15, 1989 (Toronto, Canada).

[4] For example, see *Adv. Batt. Technology 25*, No. 10, Page 4, (1989).

[5] D.P. Wilkinson, J.R. Dahn, U. von Saken and D.T. Fouchard, Paper #53 presented at the *Electrochemical Society Fall Meeting*, Seattle, Washington, U.S.A. Oct. 14~19 (1990); U.von Saken and J.R. Dahn, Paper 54, ibid.

[6] T. Nagaura and K. Tozawa, *Prog. Batts. Sol. Cells 9*, 209 (1990).

[7] J.R. Dahn, U.von Sacken, M.W. Juzkow and H. Aljanaby, *J. electrochem. Soc. 138*, 2207 (1991).

[8] D. Guyomard and J.M. Tarascon, *J. electrochem. Soc. 139*, 937 (1992).

[9] G. M. Jenkins, K.Kawamura, *Polymeric Carbons - Carbon Fiber, Glass and Char*, (1976).

[10] Peter A. Thrower, Editor, *Chemistry and Physics of Carbon, Vol. 22*, 1 (1989).

[11] P.B. Hirsch, *Proc. Roy. Soc. A, Vol. 226, 143* (1954).

[12] M. Inagaki, A. Oberlin, and S.de Fonton. *High Temp. High Press. 9:453* (1977).

[13] Peter A. Thrower, Editor, *Chemistry and Physics of Carbon, Vol. 7, 237,* (19).

[14] J. E. Fischer, *Chemical Physics of Intercalation, 59,* Edited by A.P. LeGrand and S.Flandrois, (1987).

[15] V.A.Nalimova, D. Guerard, M. Lelaurain and O.V. Fateev, *Carbon 33*, in press (1995).

[16] M. S. Dresslelhaus and M. Endo, *Graphite Intercalation compounds II, ,347,* H.Zabel and S. A. Solin, Editor, (1992).

[17] J. R. Dahn, Rosamaria Fong and M.J. Spoon, *Phys. Rev. B42, 6424* (1990).

[18] Hang Shi, *Disordered Carbons and Battery Applications, Ph. D. thesis,* Simon Fraser University, (1993).

[19] Tao Zheng, Yinghu Liu, E.W. Fuller, Sheilla Tseng, U. von Sacken and J.R. Dahn, *J. Electrochem. Soc.,* accepted April, 1995.

[20] Tao Zheng, J. N. Reimers, J. R. Dahn, *Phys. Rev. B,* Vol. 51(2), 734, (1995).

[21] B.M. Way and J. R. Dahn, *J. Electrochem. Soc. 141, 907* (1994).

[22] For example, see A. M. Wilson and J. R. Dahn, *Canadian Patent* Application #81,

J. Electrochem. Soc., Vol. 142, No. 2, P326, February 1995,

or J. Appl. Phys. 77(6), P2363, March 1995.

[23] A. Omaru, H. Azuma, M. Aoki, A. Kita and Y. Nishi, Paper #25, *Extended Abstracts of Battery Division,* p34. Meeting of the Electrochemical Society, Toronto, Canada (1992).

[24] Data from *Mitsubishi Gas Chemical Planning and Development Section, New Business Division.*

[25] *Encyclopedia of Polymers and Plastics, Vol.6, Epoxy Resins,* p231.

[26] Manual from the company, *General Guide, Formulating with Dow Epoxy Resin..*

[27] W.J. Weydanz, B.M. Way, T. van Buuren and J.R. Dahn, *J. Electrochem. Soc., Vol 141, No. 4, 900* (1994).

[28] B. D. Cullity, *Elements of X-ray Diffraction,* (1956).

[29] J. D. Bernal, *Proc. Roy. Soc. London A 106,* 749, (1924).

[30] B. E. Warren, *Phys. Rev. 59, 693*, (1941).

[31] Kim Kimoshita, *Carbon, Electrochemical and Physicochemical Properties*, John Wiley & Sons (1988).

[32] V. A. Drits, and C. Tchoubar, *X-ray Diffraction by Disordered Lamellar Structures*, Springer-Verlag, (1991).

[33] Hang Shi, J. N. Reimers and J. R. Dahn, *J. Appl. Crystallography 26*, 827 (1993).

[34] W.R. Mckinnon and R.R. Haering, *Modern Aspects of Electrochemistry*, Vol. 15, ed. R.E. White, J.O'M. Bockris and B.E. Conway, N.Y.Plenum (1982).

[35] Z.X. Shu, R.S. McMillan and J.J. Murray, *J. Electrochem. Soc. 140*, 922 (1993).

[36] Rosamaria Fong, Ulrich von Sacken and J.R. Dahn, *J. Electrochem. Soc., Vol 137, No. 7, 2009*, (1990).

[37] J.R. Dahn, Tao Zheng, Yinghu Liu and J.S. Xue, Submitted to Science, April 7, 1995.

[38] K. Sato, M. Noguchi, A. Demachi, N. Oki and M. Endo, *Science 264*, 556 (1994).

[39] A. Mabuchi, K. Tokumitsu, H. Fujimoto and T. Kasuh, *7th International Meeting on Lithium Batteries, May 15-20*, (1994), Boston, Massachusetts, U.S.A., paper I-A-10, page 207 of extended abstracts; also see H.Fujimoto, A. Mabuchi, K. Tokumitsu and T. Kasuh, ibid, paper II-B- 12, page 540.

[40] Toshiako Enoki, *J. Mater. Res. Vol 5, No. 2*, Feb. (1990).

[41] For example, hysteresis in Li electrochemical cells was observed when Mo-S bonds in $LiMoS_2$ were broken due to the formation of Li-S bonds upon further insertion of lithium - see L.S. Selwyn, W.R. McKinnon, U. von Sacken and C.A. Jones, *Solid State Ionics 22, 337* (1987).

[42] J.E. Fisher, in *Chemical Physics of Intercalation*, edited by A.P. Legrand and S. Flandrois (Plenum, New York, 1987).

[43] J.R. Dahn, *Phys. Rev. B44, 9170* (1991).

[44] M.Ishikawa, N. Sonobe, H. Chuman and T. Iwasaki, *35th Battery Symposium in Japan*, Nov. 14-16 (1994), Nagoya, Japan, paper 2B10, extended abstracts, page 49.

[45] Yinghu Liu, J.S. Xue, Tao Zheng and J.R. Dahn, submitted to carbon, April 1995.